NASA/CR—1999-208877

Source Methodology for Turbofan Noise Prediction (SOURCE3D Technical Documentation)

Harold D. Meyer
United Technologies Corporation, Windsor Locks, Connecticut

Prepared under Contract NAS3–26618

National Aeronautics and
Space Administration

Glenn Research Center

March 1999

Acknowledgments

The author would like to thank Donald B. Hanson and David A. Topol of Pratt & Whitney for their helpful suggestions and critiques. Also, appreciation is due to Donald B. Hanson for suggesting this project and for his contributions to theory which have been acknowledged in the text where appropriate. Additionally, thanks should be given to Dennis L. Huff of NASA Lewis Research Center for his support.

Available from

NASA Center for Aerospace Information
7121 Standard Drive
Hanover, MD 21076
Price Code: A05

National Technical Information Service
5285 Port Royal Road
Springfield, VA 22100
Price Code: A05

TABLE OF CONTENTS

	Page
LIST OF SYMBOLS	iv
LIST OF FIGURES	x
SUMMARY	xi
CHAPTER 1: INTRODUCTION	1
CHAPTER 2: PRELIMINARIES	4
2.1 Geometry and Definition of Swirl	4
2.2 Standard Waves and Source Vector/Scattering Coefficient Definition	8
CHAPTER 3: SOURCE VECTOR COEFFICIENTS AND SCATTERING COEFFICIENTS FOR THE STATOR AND ROTOR ALONE	13
3.1 Upwash and Loading	13
3.2 Source Vector Coefficients and Scattering Coefficients	20
CHAPTER 4: ADDITIONAL THEORY	25
4.1 Flow Turning at the Stator and Rotor	25
4.2 Combined Elements	29
CHAPTER 5: CONCLUDING REMARKS	30

APPENDIX A: PRESSURE MODAL AMPLITUDES FOR A SYSTEM WITH SWIRL 32

APPENDIX B: VORTICITY WAVE MODAL AMPLITUDES 42

APPENDIX C: SCATTERING COEFFICIENTS FOR ACTUATOR DISKS 49

APPENDIX D: COMBINING STATOR OR ROTOR WITH AN ACTUATOR DISK 60

REFERENCES 66

ACKNOWLEDGMENTS 68

LIST OF SYMBOLS

$\boldsymbol{A}$ ..... state vector array

$\boldsymbol{A}^P$ ..... subvector of state vector $\boldsymbol{A}$ at interface P

A_1, A_2, A_3 ..... pressure amplitudes (see Fig. 4.2)

$\boldsymbol{A}_{in}$ ..... vector composed of input state vector coefficients [Eq. (4.2)]

$\boldsymbol{A}_{out}$ ..... vector composed of output state vector coefficients [Eq. (4.2)]

$\boldsymbol{A}_{in}^P$ ..... subvector of state vector $\boldsymbol{A}_{in}$

$\boldsymbol{A}_{out}^P$ ..... subvector of state vector $\boldsymbol{A}_{out}$

$\boldsymbol{A}_W^P$ ..... subvector of state vector $\boldsymbol{A}$ for wave type W at interface P

A_{Wskn}^P ..... state vector element (sometimes P or W may be omitted but implied)

a_∞ ..... far-field speed of sound (used for normalization)

B ..... number of rotor blades

$\boldsymbol{B}$ ..... source vector array

$\boldsymbol{B}^P$ ..... subvector of source vector $\boldsymbol{B}$ at interface P

$\boldsymbol{B}_{COMB}$ ..... combined stator/actuator disk source vector

$\boldsymbol{B}_W^P$ ..... subvector of source vector $\boldsymbol{B}^P$ for wave of type W at interface P

B_{Wskn}^P ..... source vector element (sometimes P or W may be omitted but implied)

b ..... vane semi-chord

b_R ..... rotor semi-chord

b_T ..... vane semi-chord at the tip

$\tilde{b}$ ..... $b / 2b_T$

$C_{Wskn}(r)$ ..... function used in specifying pressure modal amplitudes

c ..... speed of sound

c_a, c_b ..... medium nominal speed of sound in region a or b

c_0 ..... medium nominal speed of sound

$D_{Wskn}(r,z)$ ..... see Eq. (A.25)

$\boldsymbol{E}$ ..... matrix used in obtaining $\boldsymbol{S}_{COMB}$ and $\boldsymbol{B}_{COMB}$

E_{Wskn}^P ..... axial location shift factor [Eq. (3.25)]

$F_{WW_i skn; sk_i n_i}^{PP_i}$ ..... axial location shift factor (for input and output wave locations) [Eq. (3.26)]

$f_{kW_i, s_i n_i}$ ..... kth Fourier harmonic of elemental blade loading function for stator produced by (s_i, k, n_i) - mode input wave

f_s ..... sth Fourier harmonic of elemental blade loading function for stator

f_{sW_i,k_in_i} ..... sth Fourier harmonic of elemental blade loading function for stator produced by (s,k_i,n_i) - mode input wave

$G(x,y,t-\tau)$ ..... Green's function

g_{1n} ..... normalization parameter [Eq. (C.28)]

g_{2n} ..... normalization parameter [Eq. (C.45)]

h ..... vane or blade spacing

i ..... $\sqrt{-1}$

$J_m(\cdot)$ ..... mth order Bessel function of the first kind

K ..... reduced frequency for stator or rotor

$\boldsymbol{K_{in}}$ ..... matrix associated with input waves, used in calculating actuator disk scattering matrix

$\boldsymbol{K_{io}} = \boldsymbol{K_{out}^{-1}}\boldsymbol{K_{in}}$ ..... actuator disk scattering matrix

$K_{ioWW_iskn;skn_i}$ ..... element of matrix $\boldsymbol{K_{io}}$

$\boldsymbol{K_{out}}$ ..... matrix associated with output waves, used in calculating actuator disk scattering matrix

$K_c(\cdot)$ ..... cascade kernel function for stator or rotor

k,k_i ..... vane passing frequency harmonic index (k is output or generic value, k_i is input value)

k_{k,s_in_i} ..... chordwise gust wavenumber for rotor produced by (s_i,k,n_i) - mode input wave

k_{mnk} ..... see p. 38

k_{mns} ..... see Eq. (A.10)

k_s ..... chordwise gust wavenumber for stator

$k_{mn}(\omega)$ ..... see Eq. (A.4)

k_{s,k_in_i} ..... chordwise gust wavenumber for stator produced by (s,k_i,n_i) - mode input wave

$\tilde{k}_{skn}$ ..... $k_{skn}r_D$

L ..... number of duct sub-annuli

M ..... duct axial flow Mach number

M_{rR} ..... Mach number for rotor relative flow

M_{rS} ..... Mach number for stator relative flow

M_S ..... duct axial flow Mach number in stator region

M_{sP} ..... swirl rotational Mach number at the rotor tip at interface P

M_T ..... rotor blade tip rotational Mach number

$m = sB - kV$ ..... circumferential wavenumber of acoustic duct mode

N_1 ..... number of radial modes for wave type $W = 1$

N_2 ..... number of radial modes for wave type $W = 2$

N_3 ..... number of radial modes for wave type $W = 3$

n, n_i ..... duct radial mode index (n is output or generic value, n_i is input value)

$\boldsymbol{n}$ ..... unit outward normal to vane or blade surface

$\hat{\boldsymbol{n}}$ ..... unit outward normal to vane or blade mean surface (see Fig. 2.3)

$\boldsymbol{I}$ ..... identity matrix

P, P_i ..... index specifying an interface location or a region, see Figs. 1.1, 3.1 (P is output or generic value, P_i is input value)

p ..... acoustic pressure

p_a ..... mean pressure in region a

p_{Wskn} ..... duct mode complex harmonic pressure amplitude for wave of type W

p_W^P ..... acoustic pressure for wave of type W at interface P

p_∞ ..... far-field pressure (used for normalization)

$\tilde{p}_a, \tilde{p}_b$ ..... disturbance pressure in region a or b (Appendix C)

r ..... radial coordinate

r_D ..... duct outer radius

r_H ..... duct inner radius

r_l ..... radial coordinate value at lth radial station

$\boldsymbol{S}$ ..... scattering matrix

$\boldsymbol{S}_{COMB}$ ..... combined stator/actuator disk or rotor/actuator disk scattering matrix

S_M ..... vane or blade mean surface

$\boldsymbol{S}_{WW_i}^{PP_i}$ ..... submatrix of scattering matrix $\boldsymbol{S}$ for input wave of type W_i at interface P_i and output wave of type W at interface P

$S_{WW_i skn;s_i k_i n_i}^{PP_i}$ ..... scattering matrix element (sometimes P or W may be omitted but implied)

$S(\mathbf{y})$ ..... vane or blade surface (both upper and lower)

s, s_i ..... blade passing frequency (BPF) harmonic index (s is output or generic value, s_i is input value)

t ..... time variable

U ..... axial component of mean flow

$\boldsymbol{U} = (U, V, 0)$ ..... mean velocity

U_a, U_b ..... axial component of mean velocity in region a or b

U_R, U_S ..... axial component of mean velocity in rotor and stator regions

U_{rR}, U_{rS} ..... fluid velocity relative to rotor or stator

$U_n^P(r)$ ..... vorticity wave radial duct mode (sometimes P may be omitted but implied)

$\boldsymbol{u}$ ..... disturbance velocity

u ..... axial component of disturbance velocity

u_W^P ..... axial component of disturbance velocity for wave of type W at interface P

u_{Wskn}^P ..... duct mode complex harmonic axial velocity amplitude for wave of type W at interface P

$\tilde{u}_a, \tilde{u}_b$ ..... axial component of disturbance velocity in region a or b (Appendix C)

$\tilde{u}_3$ ..... function given by S. N. Smith

$\bar{u}_{sk}(r)$ ..... see Eq. (B.3)

V ..... number of vanes, or when used in a velocity context, the transverse component of mean flow

V_a, V_b ..... transverse component of mean velocity in region a or b

v ..... transverse component of disturbance velocity

v_W^P ..... transverse component of disturbance velocity for wave of type W at interface P

v_{Wskn}^P ..... duct mode complex harmonic transverse velocity amplitude for wave of type W at interface P

$\tilde{v}_a, \tilde{v}_b$ ..... transverse component of disturbance velocity in region a or b (Appendix C)

W, W_i ..... index specifying wave type, W or W_i = 1: upstream pressure, = 2: downstream pressure, = 3: downstream vorticity (W is output or generic value, W_i is input value)

W ..... wake velocity downstream of rotor (Fig. 2.1)

W_s ..... Fourier coefficient of W

w ..... stator or rotor upwash

w_s ..... Fourier coefficient of w for stator

w^s ..... sth harmonic of upwash

w_{kW_i,s_in_i} ..... Fourier coefficient of w for rotor produced by (s_i,k,n_i)-mode input wave for input wave of type W_i

w_{sW_i,k_in_i} ..... Fourier coefficient of w for stator produced by (s,k_i,n_i)-mode input wave for input wave of type W_i

$\tilde{w}_{kW_i,s_in_i}$ ..... see Eqs. (3.11) and (3.12)

$\tilde{w}_{sW_i,k_in_i}$ ..... see Eqs. (3.18) and (3.19)

$X_{mn} = \kappa_{mn} r_D$ ..... duct radial eigenvalue (non-dimensional)

$x = (x_1, x_2, x_3)$ ..... Cartesian coordinate system for rotor/stator system. Origin may vary for different situations (Fig. 2.1)

x ..... axial coordinate (Appendix B, S. N. Smith notation), $x = r / r_D$ (Section 3.2 only)

x_{RLED} ..... axial displacement of blade leading edge

x_S ..... $x_{SD} / 2b_T$

x_{SD} ..... axial displacement of vane leading edge

x_{SOR} ..... $x_{SPAC} / 2b_T$

x_{SPAC} ..... blade trailing edge to vane leading edge axial distance

$x_{SPAC,H}$ ..... blade trailing edge to vane leading edge axial distance at the hub

x^P ..... axial interface locations (Figs. 1.1, 3.1, D.1, D.2)

x^R ..... axial location where rotor leading edge intersects the hub

x^S ..... axial location where stator leading edge intersects the hub

$\bar{x} = (r, \bar{\phi}, \bar{x}_1)$ ..... cylindrical polar coordinate system attached to stator leading edge at each radius (Fig. B.3)

$Y_m(\cdot)$ ..... mth order Bessel function of the second kind

$y = (r', \bar{\phi}', y_1)$ ..... field point in Green's function

y ..... transverse coordinate (Appendix B, S. N. Smith notation)

y_{RD} ..... azimuthal displacement of blade trailing edge

y_{RLED} ..... azimuthal displacement of blade leading edge

y_S ..... $y_{SD} / 2b_T$

y_{SD} ..... azimuthal displacement of vane leading edge

z ..... chordwise coordinate along the vane or blade

z_0 ..... vane chord coordinate (Appendix B, S. N. Smith notation)

z' ..... observer chordwise coordinate along the vane or blade

$\mathbf{0}$ ..... zero matrix

α_{CL} ..... blade relative velocity flow angle

$\alpha_{CL,H}$ ..... blade relative velocity flow angle at the hub

α_R ..... negative of blade stagger angle

α_S ..... vane stagger angle

α_3 ..... axial wavenumber (Appendix B, S. N. Smith notation)

β ..... $\sqrt{1-M_r^2}$. Also, transverse wavenumber (Appendix B only, S. N. Smith notation)

β_r ..... $\sqrt{1-M_{rS}^2}$ or $\sqrt{1-M_{rR}^2}$, respectively, for stator or rotor

Γ ..... parameter used in specifying $K_c(\cdot)$. Also, $\Gamma = \pi(r_D^2 - r_H^2)$ (Appendix A)

$\Gamma(z_0)$ ..... vortex strength (Appendix B, S. N. Smith notation)

$\gamma_{mn}(\omega)$ ..... see Eq. (A.3)

γ_{mnk} ..... see p. 38

γ_{mns} ..... see Eq. (A.9)

γ_{Wskn}^P ..... axial wavenumber of duct mode (sometimes P or W may be omitted but implied)

$\tilde{\gamma}_{skn}$ ..... $\gamma_{skn} r_D$

Δp ..... unsteady loading on vanes or blades

Δp_k ..... kth Fourier coefficient of unsteady loading on blades

Δp_s ..... sth Fourier coefficient of unsteady loading on vanes

Δr ..... radial increment (see Fig. B.1)

Δr_l ..... $(r_l - r_{l-1})$, radial increment at radial station l (see Fig. B.1)

$\delta(\cdot)$ ..... Dirac delta function

$\delta_{n,n'}$ ..... Kronecker delta

$\delta_{1n,n'}$ ..... see Eq. (C.33)

$\delta_{2n,n'}$ ..... see Eq. (C.50)

$\delta_{3n,n'}$ ..... see Eq. (C.51)

∇ ..... gradient operator

∇_y ..... gradient operator evaluated with respect to field point coordinates y

θ ..... stagger angle (Appendix B, S. N. Smith notation)

κ_{mn} ..... duct mode radial eigenvalue (dimensional)

λ^P_{Wskn} ..... see Eq. (C.9)

$\tilde{\lambda}^P_{Wskn}$ ..... λ^P_{Wskn} / c_P, where P indicates axial interface or region

ν ..... vane or blade index

ρ, ρ_0 ..... mean fluid density

ρ_a, ρ_b ..... mean fluid density in region a or b

ρ_R, ρ_S ..... mean fluid density in rotor or stator region

σ_R ..... inter-blade phase angle

σ_S ..... inter-vane phase angle

σ_{cS} ..... $2b_T / r_D$

σ_r ..... r_H / r_D

τ ..... time variable

ϕ ..... polar angle coordinate

$\bar{\phi}, \bar{\phi}'$ ..... polar angle coordinate for field and source points, respectively, in inertial reference coordinate system

ϕ' ..... polar angle coordinate for source point in stator-fixed coordinate system

$\hat{\phi}'$ ..... polar angle coordinate for source point in rotor-fixed coordinate system

$\psi^P_{mn}(r)$ ..... duct acoustic wave radial mode (sometimes P or W may be omitted but implied)

$\Omega = (\Omega_1 - \Omega_2)$ ..... actual rotor rotational speed

Ω_s ..... swirl flow rotational speed

Ω_{sa}, Ω_{sb} ..... swirl flow rotational speed in region a or b

Ω_1 ..... rotor rotational speed with respect to inertial coordinate system (Fig. 2.3)

Ω_2 ..... stator rotational speed with respect to inertial coordinate system (Fig. 2.3)

ω ..... radian frequency

LIST OF FIGURES

Page

Figure 1.1. Acoustic Elements for a Turbofan Engine. 2

Figure 2.1. Rotor/Stator Geometry. 5

Figure 2.2. Blade/Vane Geometry. 6

Figure 2.3. Rotor/Stator Schematic. 7

Figure 3.1. Axial Interface Coordinates at the Hub. 22

Figure 4.1. Flow Turning at Rotor and Stator. 26

Figure 4.2. The Three Possible Types of Scattering Interaction. 27

Figure A.1. Stator Geometry for Acoustic Wave Modal Analysis. 34

Figure A.2. Rotor Geometry for Acoustic Wave Modal Analysis. 39

Figure B.1. Geometry for Subdivided Annular Duct. 43

Figure B.2. Two-Dimensional Stator Cascade. 44

Figure B.3. Stator Geometry for Vorticity Wave Modal Analysis. 46

Figure C.1. Setup for the Actuator Disk Derivation. 50

Figure D.1. Combining the Stator Alone and Actuator Disk into One Element. 61

Figure D.2. Combining the Rotor Alone and Actuator Disk into One Element. 65

SUMMARY

This report provides the analytical documentation for the SOURCE3D Rotor Wake/Stator Interaction Code. It derives the equations for the rotor scattering coefficients and stator source vector and scattering coefficients that are needed for use in the TFaNS (Theoretical Fan Noise Design/Prediction System). Source vector coefficients are the coefficients for stator scattering of rotor wakes into acoustic and vortical waves. Scattering coefficients are the reflection and transmission coefficients for the rotor and stator for inputs of unit amplitude acoustic or vorticity waves. SOURCE3D treats the rotor and stator as isolated source elements. TFaNS uses this information, along with scattering coefficients for inlet and exit elements, and provides complete noise solutions for turbofan engines.

In the past, three-dimensional source codes, generally, have only treated noise produced by the rotor wake interacting with the stator. Reflection and transmission from the rotor has been ignored. Also, vorticity waves and the effect of swirl have been omitted. These items are needed to account for frequency scattering and mode trapping. Frequency scattering is the phenomenon where the rotor scatters an input wave at blade passing frequency (BPF) into other harmonics. Mode trapping is the mechanism whereby the BPF mode reflects back and forth between the rotor and stator, then finally scatters into higher harmonics, and exits.

SOURCE3D is composed of a collection of FORTRAN programs that have been obtained by extending the approach of the earlier V072 Rotor Wake/Stator Interaction Code. Similar to V072, it treats the rotor and stator as a collection of blades and vanes having zero thickness and camber contained in an infinite hard-walled annular duct. Acoustic and vorticity waves are calculated by distributing pressure dipoles on the blades and vanes. Then acoustic wave amplitudes are calculated at arbitrary points within the duct using the normal mode expansion of the Green's function for an annular duct; vorticity wave amplitudes are calculated via a strip application of S. N. Smith's cascade theory.

SOURCE3D adds important features to the V072 capability – a rotor element, swirl flow and vorticity waves, actuator disks for flow turning, and combined rotor/actuator disk and stator/actuator disk elements. These items allow reflections from the rotor, frequency scattering, and mode trapping, thus providing more complete noise predictions than previously. The code has been thoroughly verified through comparison with D. B. Hanson's CUP2D two-dimensional coupled cascade noise prediction code using a narrow annulus test case. For this case, which provides a two-dimensional situation, our results were essentially identical.

CHAPTER 1

INTRODUCTION

In turbofan noise prediction programs such as the V072 Rotor Wake/Stator Interaction Code (Ref. 1), rotor wakes impinge on the stator producing unsteady vane loads that cause noise. Generally in these codes, reflections from other fan elements are ignored. However, reflections from the inlet, exit, and rotor could affect source strength. Experimental studies by Topol, Holhubner, and Mathews (Ref. 2) have shown this to be the case. Also, Hanson has demonstrated this analytically using his coupled cascade theory (Ref. 3) and Meyer (Ref. 4) has shown that inlet reflections coupled with the stator can have an impact on source noise levels. It was shown in Ref. 3 that such such reflections are necessary for accurate noise predictions; also that a swirl component of mean flow and vorticity waves must be included. These additions to the acoustic models account for mode trapping and frequency scattering which contribute to improved correlation with empirical results. Mode trapping is the phenomenon, described by Hanson (Ref. 3), where a mode at blade passing frequency (BPF) reflects back and forth between the rotor and stator, but is cut off in the inlet and exit. Scattering, i.e. frequency scattering, of this mode by the rotor produces higher harmonic modes which then escape through through the inlet or exit. The presence of swirl between the rotor and stator provides a speed range where mode trapping occurs.

The TFaNS (Theoretical Fan Noise Design/Prediction System, Ref. 5), developed by Pratt & Whitney under contract to NASA Lewis, seeks to overcome the shortcomings of earlier noise prediction systems by including unsteady coupling between four acoustic elements – inlet, rotor, stator, exit – shown in Fig. 1.1. It extends the two-dimensional approach developed by Hanson in Ref. 3, coupling the fan elements via the duct eigenmodes.

In TFaNS, the acoustic elements are coupled at the three interface planes shown in Fig. 1.1. The axial coordinate is x_1 and the axial locations of the interface planes are at x^1, x^2, x^3. At these planes, state vector $\boldsymbol{A}$ with elements $\boldsymbol{A}^1$, $\boldsymbol{A}^2$, and $\boldsymbol{A}^3$, and source vector $\boldsymbol{B}$ with elements $\boldsymbol{B}^1$, $\boldsymbol{B}^2$, and $\boldsymbol{B}^3$, are defined. The state vector elements $\boldsymbol{A}^1$, $\boldsymbol{A}^2$, and $\boldsymbol{A}^3$ give the pressure modal amplitudes for acoustic waves and velocity modal amplitudes for vorticity waves. The source vector elements $\boldsymbol{B}^1$, $\boldsymbol{B}^2$, and $\boldsymbol{B}^3$ give the pressure modal amplitudes for the acoustic waves generated by the rotor wake impinging on the stator. These elements also give the velocity modal amplitudes for the vorticity waves generated by this wake. State vectors and source vectors will be described later, in more detail, in Section 2.2.

The action, in TFaNS, of the rotor wake impinging on the stator to create waves that pass back and forth between the various elements to produce the final noise, is described by the system of equations

$$\boldsymbol{A} = \boldsymbol{S}\boldsymbol{A} + \boldsymbol{B}, \tag{1.1}$$

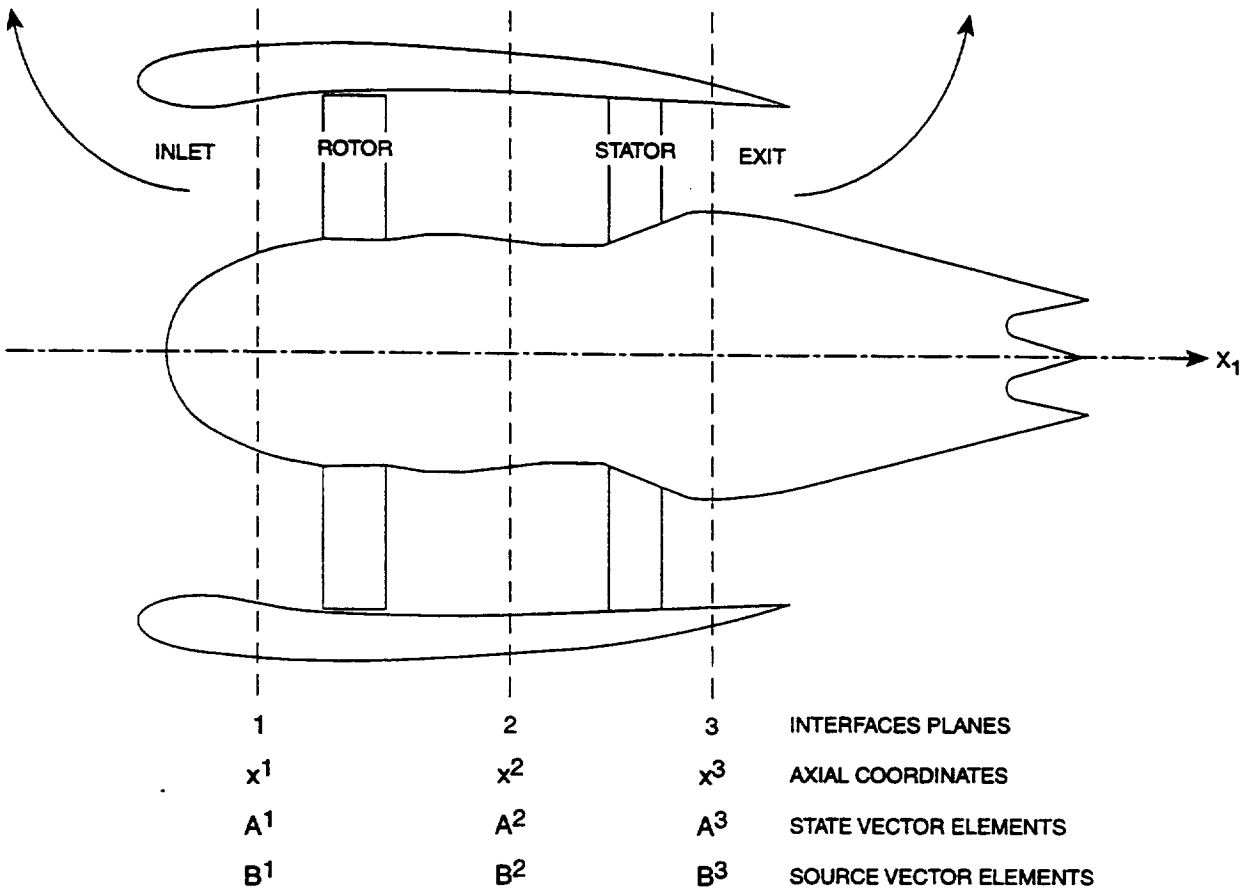

FIGURE 1.1 ACOUSTIC ELEMENTS FOR A TURBOFAN ENGINE

where S is a scattering matrix made up of modal reflection and transmission coefficients at the various interfaces. The scattering coefficients will be described in more detail later. Solving this equation gives the state vector

$$A = (I - S)^{-1} B, \tag{1.2}$$

which can then be used to calculate sound power levels and other desired acoustic information.

At the heart of the TFaNS system is the SOURCE3D Rotor Wake/Stator Interaction Code which calculates the matrix S and vector B needed for the equations above by treating the stator and rotor source elements each in isolation. The purpose of this report is to document the approach used by SOURCE3D in attaining this goal.

SOURCE3D was developed at Hamilton Standard; it is coded in FORTRAN 77 and was designed for UNIX™ workstations. It uses the basic framework provided by V072 and retains much of that code. The basic physical and geometric assumptions for SOURCE3D are the same as those for V072. In particular, SOURCE3D treats unsteady, subsonic, isentropic flow in an annular, infinite duct. There is a background of uniform mean flow in each of the element regions. The stator vanes and rotor blades are treated as flat plates with negligible camber and thickness. Ref. 1 provides further details regarding basic assumptions.

SOURCE3D is significantly different from V072 in that it treats both the stator and the rotor, rather than just the stator. Also, it calculates source vector coefficients and scattering coefficients, rather than the pressure modal amplitudes computed by V072. Additionally, solid body swirl has been added to the mean flow between the rotor and stator, along with actuator disks to implement the flow turning accompanying the swirl. These disks turn the flow at the upstream edge of the rotor and straighten it at the furthest trailing point of the stator. Only acoustic waves were included in V072. SOURCE3D adds vorticity waves and the source vector coefficients and scattering coefficients associated with these. Rather than treat the stator and its actuator disk as separate acoustical elements, SOURCE3D first treats these individually, then combines them into a single element. The same is true for the rotor and its actuator disk. Acoustic wave source vector coefficients and scattering coefficients are computed in much the same way that V072 (Ref. 1) determines modal pressure amplitudes. It calculates vorticity wave type source vector coefficients and scattering coefficients much the same as modal amplitudes are computed in Smith (Ref. 6). In order to provide the features mentioned above, much new code and numerous new subroutines have been added to V072. Additionally, many portions of the old code have been modified.

CHAPTER 2

PRELIMINARIES

Before deriving, in the next chapter, source vector coefficients and scattering coefficients for the stator and rotor, we need to provide some preliminary information. The first section of this chapter treats geometry and provides a definition of swirl by means of a coordinate system transformation. Much of this is repeated from Ref. 1, but in less detail; the swirl part is new. Standard waves, source vector coefficients, and scattering coefficients are defined in the second section. The standard waves provide the form of the input and output for scattering. They are also treated in Ref. 5. There is additional information about source vector coefficients and scattering coefficients in Refs. 3 and 5.

2.1 Geometry and Definition of Swirl

The rotor/stator geometry is shown in Fig. 2.1. As seen there, a cylindrical polar coordinate system is fixed in the duct with axial coordinate x_1 along the duct centerline. The coordinate x_1 increases in the direction of air flow. Depending on the context, the origin for x_1 may be different in different situations. The rotor turns with fan rotational speed Ω in the direction of increasing ϕ. The duct has inner radius r_H and outer radius r_D. The rotor is made up of B evenly spaced identical blades, and the stator consists of V evenly spaced identical vanes.

The axial and azimuthal sweep of the rotor blades and stator vanes are defined, respectively, by the parameters x_{RLED}, y_{RLED}, and x_{SD}, y_{SD} specified in Fig. 2.2. These quantities are defined relative to the leading edges of the rotor and stator at the hub. For the definition of the wake, the parameter y_{RD}, shown in Fig. 2.2 and defined relative to the rotor trailing edge at the hub, is needed. The parameter x_{SPAC}, also required for the wake, corresponds to the axial spacing between the rotor trailing edge and the stator leading edge. All these parameters are functions of radius r and are zero at the hub.

Fig. 2.3 shows an "unrolled" rotor/stator geometry, i.e., the intersection of the rotor blades and stator vanes with a cylindrical surface of radius r. In this figure, α_S is the stagger angle of the stator and α_R is the negative of the stagger angle of the rotor. Angle α_R is defined this way so that it will be the analog of α_S when switching from stator- to rotor-based derivations. The blades have spacing $2\pi r/B$, and the vanes, $2\pi r/V$. The local semi-chords of the blades and vanes are, respectively, b_R and b which are functions of r. Note that the (x_1, x_2)-axes, shown fixed to the stator, will be used later for analysis with regard to the stator. A similar coordinate system, shown fixed to the rotor, will be used later for rotor analysis. Other parameters included on the figure are there for later reference and will be introduced then. Also note that some of the parameters on Fig. 2.3 are further defined on Fig. 2.2.

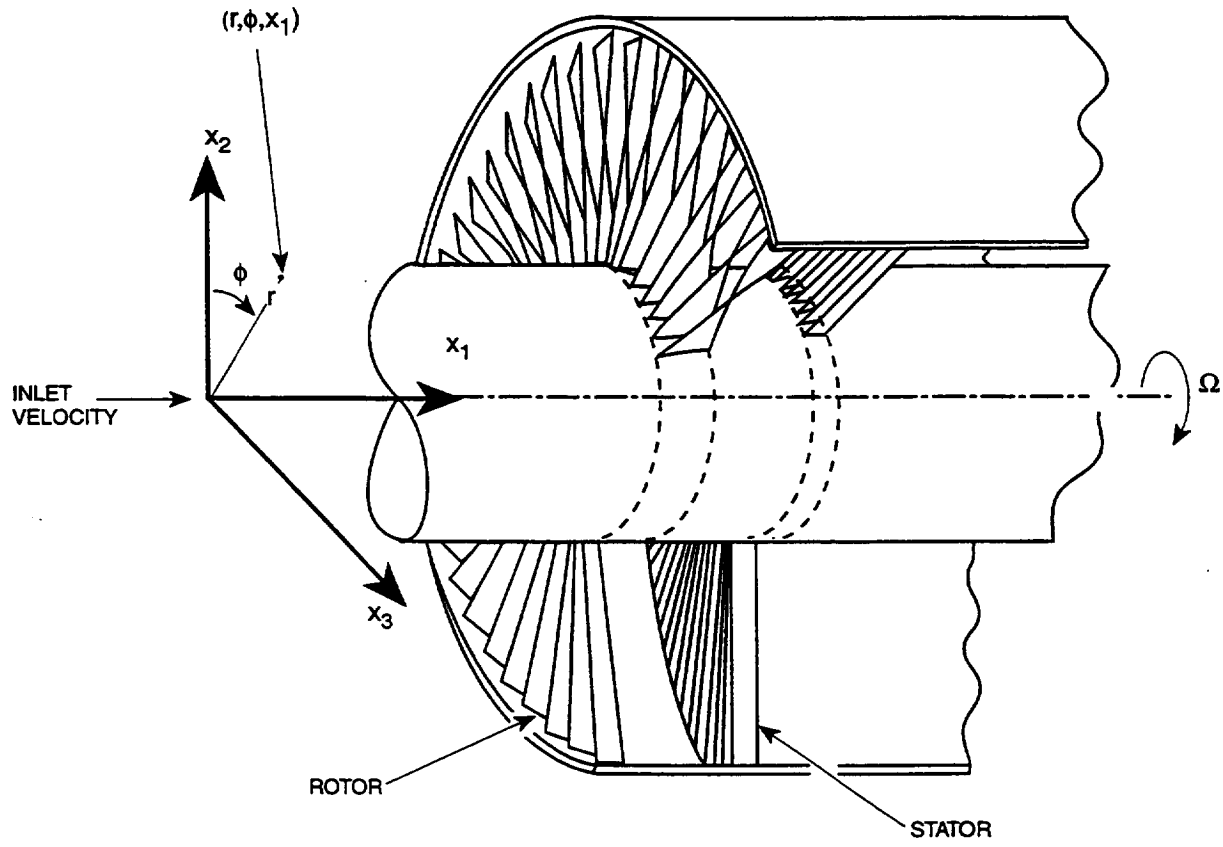

FIGURE 2.1 ROTOR/STATOR GEOMETRY

(A) DEFINITION OF y_{RLED}, y_{RD} AND y_{SD}.

SCHEMATIC VIEW OF ROTOR L.E. AND T.E.
AND STATOR L.E. LOOKING DOWN x_1 -AXIS.

y_{RD} IS POSITIVE IN THE DIRECTION OF ROTOR ROTATION.
y_{RLED} AND y_{SD} ARE POSITIVE IN THE DIRECTION OPPOSITE TO ROTOR ROTATION.

(B) DEFINITION OF x_{RLED} AND x_{SD}:

SCHEMATIC VIEW OF ROTOR L.E. AND T.E.
AND STATOR L.E. LOOKING PERPENDICULAR
TO ROTOR AXIS.

x_{RLED} IS POSITIVE WHEN THE ROTOR L.E. AT A GIVEN r IS FURTHER UPSTREAM THAN THE ROTOR L.E. AT THE HUB.
x_{SD} IS POSITIVE IN THE DIRECTION THAT REDUCES THE AXIAL SPACING RELATIVE TO THE HUB STREAMLINE.

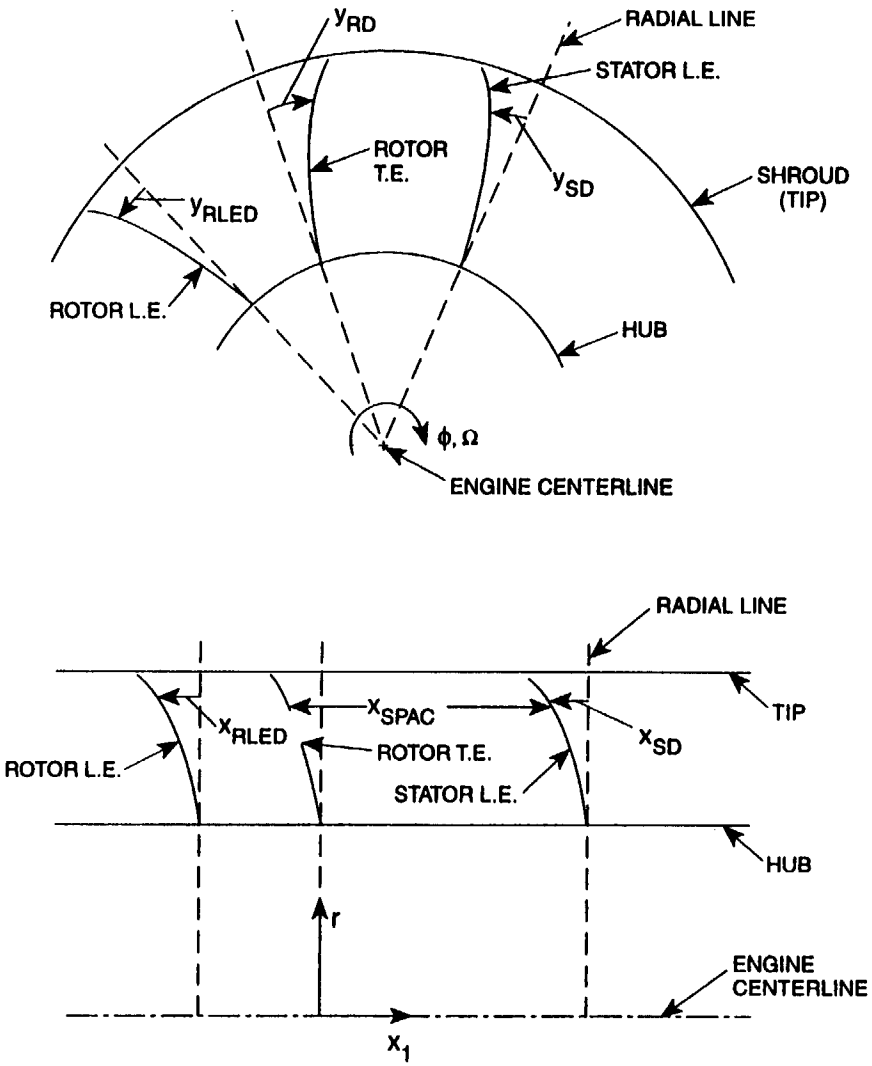

FIGURE 2.2 BLADE/VANE GEOMETRY

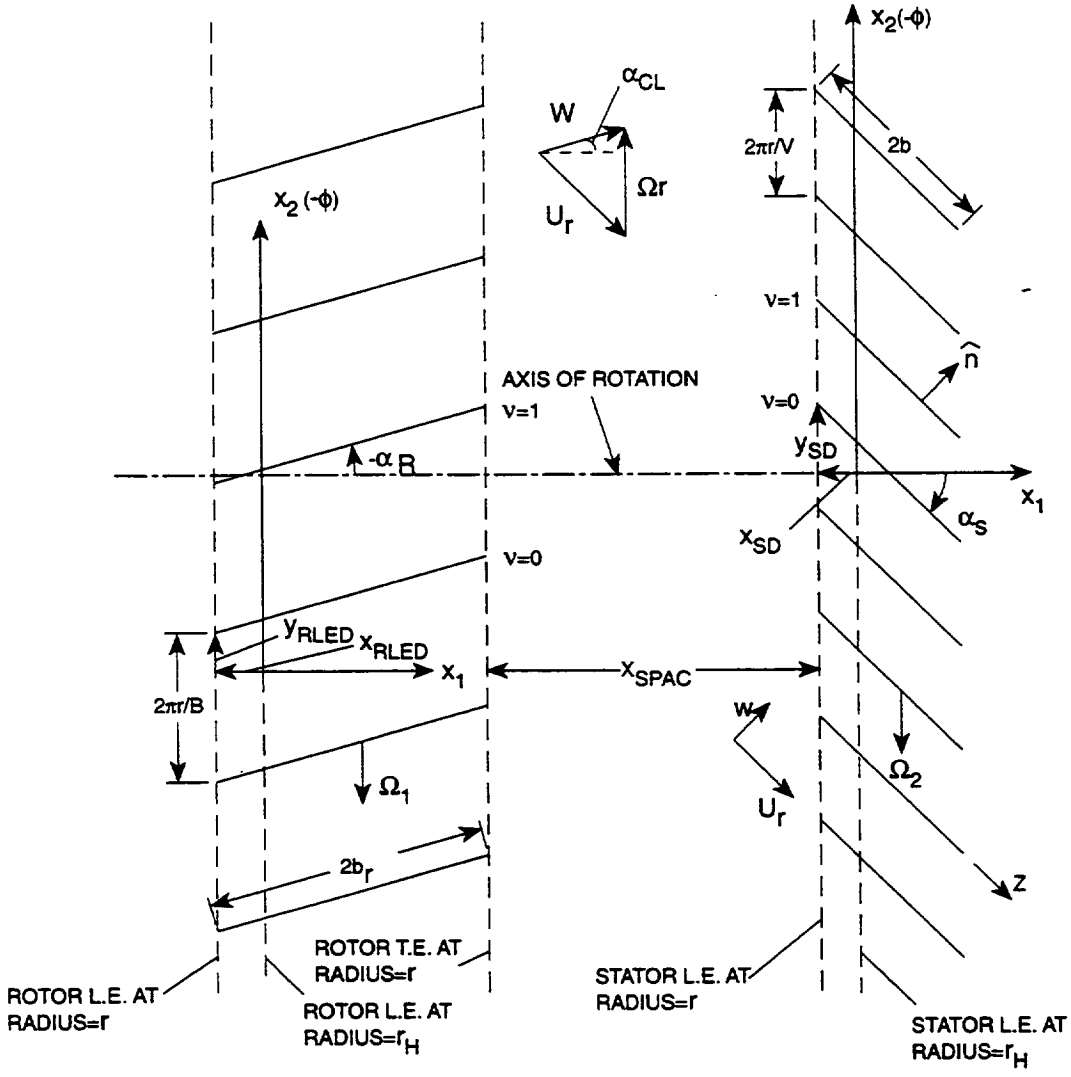

FIGURE 2.3 ROTOR/STATOR SCHEMATIC

For the case of acoustic waves, solid body swirl is approximated by rotating the stator into the approaching flow. It is introduced by using the same three-dimensional approach as in Ref. 1 only allowing both stator and rotor to rotate with speeds, respectively, of Ω_1 and Ω_2 (see Fig. 2.3). The difference in speeds corresponds to the actual rotor speed Ω. The stator speed Ω_1 corresponds to $-\Omega_s$, where Ω_s is the swirl speed.* Swirl is input by evaluating source vectors for the stator and scattering coefficients for both the stator and rotor in the stator-fixed coordinate system rather than in the inertial one. For the case of vorticity waves, the use of different coordinate systems is not necessary, because swirl is included directly, using a two-dimensional approach similar to that of Smith (Ref.6).

2.2 Standard Waves and Source Vector/Scattering Coefficient Definition

Three types of waves exist for two-dimensional duct flow (Refs. 3 and 6), upstream- and downstream-going pressure waves, and downstream-going vorticity waves. For three-dimensional flow, the physics is much more complicated and is the subject of current research (Ref. 7). However, here we take the wave families to be the upstream- and downstream-going pressure waves and two independent vorticity waves convected with the mean flow. The first vorticity wave can be defined as a wave with axial and tangential velocity components (no radial component) and corresponds to the two-dimensional vorticity wave; the second can be defined as having tangential and radial components (no axial component). The pressure waves propagate at the speed of sound; the vorticity waves are convected at the mean flow speed and do not create a pressure disturbance. At this stage of development, SOURCE3D uses only the two acoustic waves and the first vorticity wave.

These three types of waves are represented in terms of standard wave forms, which in turn are specified in terms of modal amplitudes, or applying more general terminology, state vectors. Using these quantities, we can define source vector coefficients and scattering coefficients. The standard wave forms presented in this section are those that pertain to the stator-fixed coordinate system which is the system in which all our final results are given.

Pressure waves, either upstream- or downstream-going, are represented by the expression

$$p_W^P(x_1,r,\phi,t) = p_\infty \sum_{s=-\infty}^{\infty} \sum_{k=-\infty}^{\infty} \sum_{n=1}^{\infty} A_{Wskn}^P \Psi_{mn}^P(r) e^{i\left[m\phi - \gamma_{Wskn}^P (x_1 - x^P) - sB\Omega t\right]}, \qquad (2.1)$$

where the state vector components, A_{Wskn}^P, represent the pressure modal amplitudes and are normalized by the far-field pressure, p_∞. This expression holds in the vicinity of the axial interface locations x^P, where P = 1, 2, 3 (see Fig. 1.1). The subscript W = 1 represents upstream-going pressure waves, $W = 2$ downstream-going ones. Further, s is the blade passing

* The reason for the minus is that swirl is defined as positive in the direction of positive x_2 (Fig. 2.3). However, retaining previous V072 conventions, ϕ and Ω_1 are positive in the direction of negative x_2.

frequency (BPF) harmonic index; k, the vane passing frequency harmonic index; n, the duct radial mode index;* and m is the circumferential mode order, where $m = sB - kV$. The function $\psi^P_{mn}(r)$ is the duct radial mode, γ^P_{Wskn} is the axial wavenumber,** and t is time. In the code, as would be expected, the infinite limits for s, k, n, as seen in Eq. (2.1), are truncated to give a finite number of propagating and decaying modes for the coupling analysis. The user sets the criteria for how this is done.

Note that not all of the indices appearing in the Ref. 5 version of Eq. (2.1) are present in Eq. (2.1), because the same degree of generality is not required here. Further, note that, as we proceed through this report, for convenience, we may sometimes omit some indices from symbols such as those in Eq. (2.1), when it is clear from context what these indices should be. Also, the variable x^P, when indicated, may sometimes represent locations other than those in Fig. 1.1.

The pressure in Eq. (2.1) is a linear combination of the standard modes for an annular duct with hard walls. These modes are discussed in Ref. 1 and have the general form

$$\psi_{mn}(r)e^{i(m\phi-\gamma_{skn}x_1-sB\Omega t)}. \tag{2.2}$$

The radial modes here and in Eq. (2.1) are given by

$$\psi_{mn}(r) = A_{mn}J_m(\kappa_{mn}r) + B_{mn}Y_m(\kappa_{mn}r), \tag{2.3}$$

where J_m and Y_m are Bessel functions of the first and second kind, and κ_{mn} is the duct mode radial eigenvalue. The duct mode amplitudes A_{mn} and B_{mn} are chosen so that the maximum value of ψ_{mn} over r is +1. Further, the axial wave numbers are given by

$$\gamma_{skn} = \frac{1}{\beta^2}\left[M\left(\frac{sB\Omega - m\Omega_s}{c_0}\right) \pm k_{skn}\right], \tag{2.4}$$

where the (+)-sign is for upstream-going waves ($W = 1$) and the (-)-sign is for downstream-going ones ($W = 2$). Also, c_0 is the speed of sound; M is the axial flow Mach number, U/c_0, where U is the duct uniform axial velocity; $\beta = \sqrt{1-M^2}$; and

---

* Consistent with the convention in V072, radial mode indices here start at 1. However, in conformance with standard practice, when output is printed, SOURCE3D adjusts this index to begin instead at 0.

** These wavenumbers are the negative of those specified for TFaNS in Ref. 5. However, the source vector coefficients and scattering coefficients calculated will be the same because the sign in front of γ^P_{Wskn} in Eq. (2.1) is minus (-) and it is plus (+) in TFaNS documentation. SOURCE3D utilizes the present convention in order to maintain consistency with V072.

$$k_{skn} = \sqrt{\left(\frac{sB\Omega - m\Omega_s}{c_0}\right)^2 - \beta^2 \kappa_{mn}^2}\,. \tag{2.5}$$

Note that Eqs. (2.4) and (2.5) differ from the analogous expressions in Ref. 1 in that, now, terms $m\Omega_s$ appear due to swirl. The analysis later in Appendix A will show why this is the case. Additionally, the notation has been modified so that k replaces m as a subscript, where m, as before, is given by $m = sB - kV$.

Standard vorticity waves will be represented here using the axial disturbance velocity component u_W^P. All other information, such as the transverse component, will be derivable from this. This component is given by an expression analogous to that for pressure,

$$u_W^P(x_1, r, \phi, t) = a_\infty \sum_{s=-\infty}^{\infty} \sum_{k=-\infty}^{\infty} \sum_{n=1}^{\infty} m A_{Wskn}^P U_n^P(r) e^{i\left[m\phi - \gamma_{Wskn}^P (x_1 - x^P) - sB\Omega t\right]}. \tag{2.6}$$

Here W = 3, and the normalization parameter a_∞ is the far-field speed of sound. The state vector, A_{Wskn}^P, represents the axial velocity mode amplitude u_{Wskn}^P divided by m, and the $U_n^P(r)$ are the duct radial mode functions associated with the vorticity waves. The normalization by m in A_{Wskn}^P is needed to eliminate undesired division by 0 when m = 0 in some of the actuator disk formulas which are derived later. Note that the $U_n^P(r)$'s are not the solutions of a particular differential equation associated with this analysis, but are an orthogonal basis set convenient for use here.

Similar to the case for pressure waves, the axial velocity component in Eq. (2.6) is a linear combination of vorticity duct modes of the form

$$U_n(r) e^{i(m\phi - \gamma_{skn} x_1 - sB\Omega t)}, \tag{2.7}$$

where here the axial wave numbers for wave type W = 3 are given (Ref. 6) by

$$\gamma_{skn} = \frac{m\Omega_s - sB\Omega}{U}, \tag{2.8}$$

which guarantees that these waves are convected with the mean flow. The vorticity wave radial duct modes are given by

$$U_n(r) = \cos\left[\frac{(n-1)\pi(r - r_H)}{r_D - r_H}\right]. \tag{2.9}$$

The modes in Eq. (2.7) are the same as those derived and discussed in Ref. 6. However, the notation has been changed to that used here and the form is slightly modified. Also, the modes have the additional factor $U_n(r)$ because they are three-dimensional rather than two-dimensional. The particular set of functions $U_n(r)$ was chosen to have the properties expected physically for the vorticity modes; also because they provide a complete family of functions in the mathematical sense. This selection is similar to Goldstein's choice in Ref. 8, p. 223.

Before finally defining source vector coefficients and scattering coefficients, some observations about scattering should be made. As per the discussion in Ref. 3, upstream-going pressure waves will scatter into upstream- and downstream-going pressure waves and into downstream-going vorticity waves. Downstream-going pressure and vorticity waves will do the same. With regard to indices, the stator scatters input waves with indices s_i, k_i, n_i into s_i again, but not necessarily into k_i and n_i. This scattering is viewed in the stationary coordinate system, which is our stator-fixed system. The opposite is true for the rotor in the stationary coordinate system; it scatters input waves with indices s_i, k_i, n_i into k_i again, but not necessarily into s_i and k_i. Thus schematically we have

Stator: $\quad s_i, k_i, n_i \quad \rightarrow \quad s_i, k, n,$

Rotor: $\quad s_i, k_i, n_i \quad \rightarrow \quad s, k_i, n.$

Note that mode scattering for the rotor can give both positive and negative values for the output harmonic s.

In SOURCE3D, the source vector coefficients, B^P_{Wskn}, are the mode amplitudes produced by the rotor wake acting on the stator, i.e., they are the values of A^P_{Wskn} in Eqs. (2.1) or (2.6) for the output waves generated by the wake. The scattering coefficients are the mode amplitudes, $S^{PP_i}_{WW_i skn;s_i k_i n_i}$, produced by a unit modal input wave, i.e. one with $A^{P_i}_{W_i s_i k_i n_i} = 1$. Alternatively, these coefficients are the ratios $A^P_{Wskn} / A^{P_i}_{W_i s_i k_i n_i}$ for the case where the input state vector coefficients are not necessarily unity but are arbitrary. Schematically, the scattering process can be represented by the notation

$$A^P_{Wskn} \quad \leftarrow \quad S^{PP_i}_{WW_i skn;s_i k_i n_i} \; A^{P_i}_{W_i s_i k_i n_i}.$$

Clearly, the indices must conform to the input/output requirements described above.

The elements A^P_{Wskn}, B^P_{Wskn}, and $S^{PP_i}_{WW_i skn;s_i k_i n_i}$ can be used to define several vectors and matrices that are useful. The vector $\boldsymbol{A}^P_W$ is made up of elements A^P_{Wskn}, where the indices (s,k,n) range over all combinations that the program has selected as active. $\boldsymbol{B}^P_W$ is defined analogously,

and $S_{WW_i}^{PP_i}$ is the collection of elements $S_{WW_i skn;s_i k_i n_i}^{PP_i}$ over all active combinations of indices (s_i,k_i,n_i) and (s,k,n). As an illustration, consider the simple example where there are two harmonics, $s = 1$ and 2. Assume that the only active values of k and n for $s = 1$ are $(k = 1, n = 1)$. For $s = 2$, assume the active values are $(k = 1, n = 1)$ and $(k = 2, n = 1)$. Take $(P = 2, W = 1)$. Then we can write

$$A_1^2 = \begin{Bmatrix} A^2_{1,1,1,1} \\ A^2_{1,2,1,1} \\ A^2_{1,2,2,1} \end{Bmatrix}, \qquad B_1^2 = \begin{Bmatrix} B^2_{1,1,1,1} \\ B^2_{1,2,1,1} \\ B^2_{1,2,2,1} \end{Bmatrix}, \qquad S_{12}^{22} = \begin{bmatrix} S^{22}_{12,1,1,1,1;1,1,1} & \cdot & \cdot \\ \cdot & S^{22}_{12,2,1,1;2,1,1} & S^{22}_{12,2,1,1;2,2,1} \\ \cdot & S^{22}_{12,2,2,1;2,1,1} & S_{12,2,2,1;2,2,1} \end{bmatrix},$$

where the dots in the matrix for S_{12}^{22} represent zero elements. Using the vectors A_W^P and B_W^P, we can define more precisely the vectors A^P and B^P used in Fig. 1.1. They are given by

$$A^P = \begin{Bmatrix} A_1^P \\ A_2^P \\ A_3^P \end{Bmatrix}, \qquad B^P = \begin{Bmatrix} B_1^P \\ B_2^P \\ B_3^P \end{Bmatrix}.$$

These give overall vectors

$$A = \begin{Bmatrix} A^1 \\ A^2 \\ A^3 \end{Bmatrix}, \qquad B = \begin{Bmatrix} B^1 \\ B^2 \\ B^3 \end{Bmatrix}.$$

An overall scattering matrix S is also defined, whose level of inclusion of elements corresponds to A and B. It contains elements for all the input and output modes of all the active waves at all the various interfaces. It is displayed in Refs. 3 and 5. Consult these references for further details on S as well as on other items in this section.

CHAPTER 3

SOURCE VECTOR COEFFICIENTS AND SCATTERING COEFFICIENTS FOR THE STATOR AND ROTOR ALONE

In this chapter, we obtain source vector coefficients and scattering coefficients for what will be called the "stator alone" and "rotor alone" cases. These are the cases where coefficients are derived for the stator or rotor before adding mode scattering by actuator disks. Scattering coefficients for the actuator disks will be presented in Section 4.1. Then, Section 4.2 will discuss a procedure for combining these quantities with the present source vector coefficients and scattering coefficients to produce the final values for the stator and rotor elements.

The approach for finding source vector coefficients and scattering coefficients is the same as that in Meyer and Envia (Ref. 1) for obtaining acoustic wave pressure coefficients and as in Smith (Ref. 6) for determining vorticity waves. We must first derive the upwash on the stator or rotor coming from the rotor wake for source vectors or from unit modal amplitude standard waves for scattering coefficients. The upwash is the component of velocity of these inputs that is normal to the surface of the vanes or blades. Then the upwash is used to obtain the loading on the vanes or blades by solving Kernel function integral equations. In Refs. 1 and 6, the stator and rotor are modeled as linear cascades of flat plates which are divided chordwise into "strips" for the calculation. The loads take the form of dipole distributions. These loads are then coupled to the acoustic or vorticity modes to give output modal amplitudes.

This coupling is calculated using formulas for output modal amplitudes and output vorticity wave modal amplitudes that are derived in Appendices A and B. The formulas for pressure there differ somewhat from those in Ref. 1 because now there is swirl present between the rotor and stator. Also, the formulas for the vorticity wave case differ from those in Ref. 6 in that now we must modify the procedure to cover a three-dimensional rather than a two-dimensional situation.

3.1 Upwash and Loading

For the stator, the upwash w is evaluated in the stator-fixed system and, as discussed in Ref. 1, has the general form

$$w = -\sum_{s=-\infty}^{\infty} w_s e^{i(k_s z - 2\pi\nu sB/V - sB\Omega t)} \tag{3.1}$$

on vane ν, where w_s is the Fourier coefficient of w, k_s is the chordwise gust wavenumber, z is the chordwise coordinate along the vane with origin at center-chord and extending from $-b$ at the leading edge to $+b$ at the trailing edge, and ν is the vane index, $\nu = 0, \cdots, V-1$.

To determine the upwash in the form required by Eq. (2.1), we must first determine the velocity of its source – either the rotor wake or standard input waves – in the direction of the upwash, i.e. normal to the stator. Then we must transform this result to chordwise coordinates. Details for obtaining w_s and k_s for the rotor wake are given in Ref. 1 and will not be repeated here. From Ref. 1, we have for the rotor wake that

$$w_s = -W_s \sin(\alpha_S + \alpha_{CL}) e^{-i[sB(y_{RD}+y_{SD}-x_{SPAC}\tan\alpha_{CL}+x_{SPAC,H}\tan\alpha_{CL,H})/r]} \times e^{i[sBb(\sin\alpha_S+\cos\alpha_S\tan\alpha_{CL})/r]} \tag{3.2}$$

and

$$k_s = \frac{sB}{r}(\sin\alpha_S + \cos\alpha_S \tan\alpha_{CL}). \tag{3.3}$$

In the above, W_s is the Fourier coefficient of the wake velocity, W, downstream of the rotor, α_{CL} is the rotor blade relative velocity flow angle, and x_{SPAC} is the blade trailing edge to vane leading edge axial distance. The parameters α_S, y_{RD}, y_{SD}, and b have been defined previously; W_s, α_S, α_{CL}, y_{RD}, y_{SD}, x_{SPAC}, and b vary with radius r. These parameters are shown on the schematic in Fig. 2.3. There is a factor $e^{-isBx_{SPAC,H}\tan\alpha_{CL,H}/r}$ included in Eq. (3.2). This factor sets the phase in the circumferential direction so that the exponential term in Eq. (3.2) equals 1 at the stator leading edge at the hub. The subscript H in $x_{SPAC,H}$ and $\alpha_{CL,H}$ denotes that their values are taken at the intersection of the stator leading edge with the hub.

Note that SOURCE3D evaluates the wake Fourier coefficients semi-empirically using experimental data fitted to a Gaussian wake velocity profile. It allows several choices for these profiles and also allows use of models for hub and tip vortex flows. Further discussion of the wake and hub and tip vortices can be found in Refs. 1, 9, and 10.

To determine the upwash, when loading is from input waves rather than from the wake, we first obtain the upwash velocity components for each s. We start with either the standard pressure representation, Eq. (2.1), for acoustic waves or the standard axial velocity representation, Eq. (2.6), for vorticity waves. Using the momentum equations as in Appendix C, we can derive the axial, u, and transverse, v, components of acoustic velocity from Eq. (2.1). Similarly, using the mass conservation equation, again as in Appendix C, we can derive the transverse component for vorticity waves from the axial components appearing in Eq. (2.6). Once u and v are known, the upwash is found by resolving these components into a vector normal to the stator, using the relation

$$w = u \sin\alpha_S - v \cos\alpha_S. \tag{3.4}$$

The result is

$$w^s = -\frac{p_\infty}{\rho_S}\left[\frac{\frac{m_i}{r}\cos\alpha_S + \gamma_{sk_in_i}\sin\alpha_S}{sB\Omega + U_S\gamma_{sk_in_i} - m_i\Omega_s}\right]\psi_{m_in_i}(r)e^{i\left[m_i\phi - \gamma_{sk_in_i}(x_1 - x^S) - sB\Omega t\right]}A_{sk_in_i} \qquad (3.5)$$

for acoustic type waves, and

$$w^s = -a_\infty\left[r\gamma_{sk_in_i}\cos\alpha_S - m_i\sin\alpha_S\right]U_{n_i}(r)e^{i\left[m_i\phi - \gamma_{sk_in_i}(x_1 - x^S) - sB\Omega t\right]}A_{sk_in_i} \qquad (3.6)$$

for vorticity waves, where w^s represents the s^{th} harmonic of the upwash.

For the standard waves used in deriving the above relation, we have taken $x^P = x^S$ in Eqs. (2.1) and (2.6) so that the input waves, at this stage, originate at an interface located at x^S, the axial position where the stator leading edge meets the hub. For convenience, the W subscripts have been omitted from the expressions, but it should be clear where they would have been added. The $\gamma_{sk_in_i}$'s are those appropriate to the particular wave types; m_i is the input wave circumferential wavenumber. The variables ρ_S and U_S are, respectively, the mean density and the uniform axial velocity in the stator element region; the other parameters have appeared previously.

We next change from stator coordinates, x, to the chordwise coordinate, z, using the transformation

$$x_1 = x^S - x_{SD} + z\cos\alpha_S + b\cos\alpha_S, \qquad (3.7)$$

$$\phi = -\frac{y_{SD}}{r} + \frac{z}{r}\sin\alpha_S - \frac{2\pi\nu s}{V} + \frac{b\sin\alpha_S}{r}, \qquad (3.8)$$

referring to the geometry of Fig. 2.3. Then we have

$$w^s = -\frac{p_\infty}{\rho_S}\left[\frac{\frac{m_i}{r}\cos\alpha_S + \gamma_{sk_in_i}\sin\alpha_S}{sB\Omega + U_S\gamma_{sk_in_i} - m_i\Omega_s}\right]\psi_{m_in_i}(r)$$
$$\times e^{i\left[-\gamma_{sk_in_i}x_{SD} - m_iy_{SD}/r + (m_i/r)b\sin\alpha_S - \gamma_{sk_in_i}b\cos\alpha_S\right]}A_{sk_in_i} \qquad (3.9)$$
$$\times e^{i\left[\left(\frac{m_i}{r}\sin\alpha_S - \gamma_{sk_in_i}\cos\alpha_S\right)z - 2\pi\nu sB/V - sB\Omega t\right]}$$

for acoustic type waves, and

$$w^s = -a_\infty \left[r\gamma_{sk_in_i} \cos\alpha_S - m_i \sin\alpha_S \right] U_{n_i}(r)$$
$$\times e^{i[-\gamma_{sk_in_i} x_{SD} - m_i y_{SD}/r + (m_i/r) b \sin\alpha_S - \gamma_{sk_in_i} b \cos\alpha_S]} A_{sk_in_i} \tag{3.10}$$
$$\times e^{i[(\frac{m_i}{r}\sin\alpha_S - \gamma_{sk_in_i}\cos\alpha_S)z - 2\pi\nu sB/V - sB\Omega t]}$$

for vorticity waves.

By inspection of Eqs. (3.9) and (3.10), we now can write w_s and k_s. Because loading is from input waves rather than from the wake, then w_s and k_s depend on k_i and n_i in addition to s. To emphasize this dependence, we replace w_s and k_s with w_{s,k_in_i} and k_{s,k_in_i}. For input waves of acoustic type ($W = 1, 2$), we have

$$w_{s,k_in_i} = -\frac{p_\infty}{\rho_S} \left[\frac{\frac{m_i}{r}\cos\alpha_S + \gamma_{sk_in_i}\sin\alpha_S}{sB\Omega + U_S\gamma_{sk_in_i} - m_i\Omega_s} \right] \psi_{m_in_i}(r)$$
$$\times e^{i[-\gamma_{sk_in_i} x_{SD} - m_i y_{SD}/r + (m_i/r) b \sin\alpha_S - \gamma_{sk_in_i} b \cos\alpha_S]} A_{sk_in_i} \tag{3.11}$$
$$\equiv \tilde{w}_{s,k_in_i} A_{sk_in_i},$$

and for vorticity waves ($W = 3$),

$$w_{s,k_in_i} = -a_\infty \left[r\gamma_{sk_in_i} \cos\alpha_S - m_i \sin\alpha_S \right]$$
$$\times U_{n_i}(r) e^{i[-\gamma_{sk_in_i} x_{SD} - m_i y_{SD}/r + (m_i/r) b \sin\alpha_S - \gamma_{sk_in_i} b \cos\alpha_S]} A_{sk_in_i} \tag{3.12}$$
$$\equiv \tilde{w}_{s,k_in_i} A_{sk_in_i}.$$

For all three wave types,

$$k_{s,k_in_i} = \frac{m_i}{r}\sin\alpha_S - \gamma_{sk_in_i}\cos\alpha_S. \tag{3.13}$$

For the rotor, the upwash is evaluated in the rotor-fixed system where it has the general form

$$w = -\sum_{k=-\infty}^{\infty} w_{k,s_in_i} e^{i(k_{k,s_in_i} z - 2\pi\nu kV/B - kV\Omega t)} \tag{3.14}$$

for vane ν, $\nu = 0, \cdots, B - 1$. This is analogous to the representation in Eq. (3.1), only now $sB\Omega$ is replaced by $kV\Omega$, w_{k,s_in_i} and k_{k,s_in_i} are the rotor counterparts of w_{s,k_in_i} and k_{s,k_in_i}, and z is

the chordwise coordinate along the blade with origin at the center-chord and extending from $-b_R$ at the leading edge to $+b_R$ at the trailing edge. Because there are no wakes loading the rotor blades, there are only upwashes produced by standard wave type inputs. Otherwise, there would have been parameters w_k and k_k also.

We obtain the upwash in the form of Eq. (3.14) and the expressions for $w_{k,s_i n_i}$ and $k_{k,s_i n_i}$ by employing a procedure parallel to that for the stator. We start with the same expressions as derived before for the standard wave components u and v in the stator-fixed system, then shift these expressions to the rotor-fixed system using the transformation $\phi = \tilde{\phi} + \Omega t$, where temporarily $\tilde{\phi}$ is the polar coordinate in the stator-fixed system. The exponential $e^{i(m_i\tilde{\phi} - s_i B\Omega t)}$ in the expression for the standard wave in the stator-fixed system then becomes $e^{i[m_i(\phi-\Omega t)-s_i\Omega t]} = e^{i[m_i\phi-(s_iB-kV)\Omega t-s_iB\Omega t]} = e^{i(m_i\phi - kV\Omega t)}$ in the rotor-fixed system, giving the factor $e^{-ikV\Omega t}$ appearing in Eq. (3.14). Using the resulting expressions for u and v, and proceeding as in the stator case from this point forward, we then obtain relations comparable to Eqs. (3.11)-(3.13). In proceeding in this fashion, however, we use the relation

$$w = u\sin\alpha_R - v\cos\alpha_R \tag{3.15}$$

instead of Eq. (3.4) and the coordinate transformation

$$x_1 = x^R - x_{RLED} + z\cos\alpha_R + b_R\cos\alpha_R \tag{3.16}$$

$$\phi = -\frac{y_{RLED}}{r} + \frac{z}{r}\sin\alpha_R - \frac{2\pi\nu k}{V} + \frac{b_R\sin\alpha_R}{r} \tag{3.17}$$

in place of Eqs. (3.7) and (3.8), again referring to the geometry of Fig. 2.3. In Eq. (3.16), x^R is the axial location where the leading edge of the rotor meets the hub.

The end result is that for input waves of acoustic type ($W = 1, 2$), we have

$$\begin{aligned} w_{k,s_i n_i} &= -\frac{p_\infty}{\rho_R}\left[\frac{\frac{m_i}{r}\cos\alpha_R + \gamma_{s_i k n_i}\sin\alpha_R}{sB\Omega + U_R\gamma_{s_i k n_i} - m_i\Omega_s}\right]\psi_{m_i n_i}(r) \\ &\quad \times e^{i[-\gamma_{s_i k n_i}x_{RLED} - m_i y_{RLED}/r + (m_i/r)b_R\sin\alpha_R - \gamma_{s_i k n_i}b_R\cos\alpha_R]}A_{s_i k n_i} \\ &\equiv \tilde{w}_{k,s_i n_i}A_{s_i k n_i} \end{aligned} \tag{3.18}$$

and, for vorticity waves ($W = 3$),

$$w_{k,s_i n_i} = -a_\infty \left[r\gamma_{s_i k n_i} \cos\alpha_R - m_i \sin\alpha_R \right] U_{n_i}(r)$$
$$\times\, e^{i[-\gamma_{s_i k n_i} x_{RLED} - m_i y_{RLED}/r + (m_i/r) b_R \sin\alpha_R - \gamma_{s_i k n_i} b_R \cos\alpha_R]} A_{s_i k n_i} \qquad (3.19)$$
$$\equiv \tilde{w}_{k,s_i n_i} A_{s_i k n_i}.$$

Further,

$$k_{k,s_i n_i} = \frac{m_i}{r} \sin\alpha_R - \gamma_{s_i k n_i} \cos\alpha_R \qquad (3.20)$$

for all three wave types. The parameters α_R, x_{RLED}, y_{RLED}, and b_R, used above, have been defined previously; they are functions of radius. The quantities ρ_R and U_R are, respectively, the mean density and the uniform axial velocity in the rotor element region. Analogous to the situation for the stator, the input waves for the upwash calculation originate at an interface located at x^R, the axial location where the rotor leading edge intersects the hub.

Returning now to the stator, once the upwash is known, we can use the theory in Ref. 1 to find the loading. In particular, we determine $f_s(r,z)$, the s^{th} harmonic of the elemental vane chordwise loading function, which is defined in Ref. 1; refer there for more detail. We mention here only that $f_s(r,z)$ is related to the s^{th} harmonic of unsteady loading, Δp_s, on vane $\nu = 0$ through the relation $f_s(r,z) = \Delta p_s/\rho_S U_{rS} w_s$, where U_{rS} is the fluid velocity relative to the stator vanes. After $f_s(r,z)$ is determined, it can be used in formulas derived in Appendices A and B to obtain pressure and vorticity axial velocity modal amplitudes, which, in turn, give source vector coefficients and scattering coefficients.

As per the discussion in Chapter 3 of Ref. 1, $f_s(r, z)$ is determined as the solution to the integral equation

$$e^{ik_s z} = -\int_{-b}^{b} K_c(z-y) f_s(r,y) \frac{dy}{b}, \qquad (3.21)$$

where $K_c(z - y)$ is the cascade kernel function for the stator. For standard wave input rather than rotor wake input, k_s and f_s should be replaced by $k_{s,k_i n_i}$ and $f_{s,k_i n_i}$. K_c is evaluated by using the following parameters (see Ref. 1):

β_r: $\sqrt{1 - M_{rS}^2}$,

Reduced frequency: $K = -sB\Omega b / (\beta_r^2 c_S)$,

Inter-vane gap: $h = 2\pi r / V$,

Vane stagger angle: α_S,

$$\Gamma: \quad -\frac{2\pi sB}{V}[1+M_T M_{rS}(r/r_D)\sin\alpha_S/\beta_r^2].$$

In the above, c_S is the nominal speed of sound in the stator element region, M_T is the rotor blade tip rotational Mach number, and M_{rS} is the Mach number of stator relative flow, U_{rS}/c_S. The negative sign is used in Eq. (3.21) because we need the loading that induces a normal velocity equal, but opposite in sign, to the wake or standard wave input.

For the rotor, the loading function for standard waves is $f_{k,s_i n_i}(r,z)$ rather than $f_{s,k_i n_i}(r,z)$. If we proceed through the analogous steps for the rotor as previously described in Ref. 1 for the stator, we obtain the integral equation

$$e^{\bar{i}k_{k,s_i n_i} z} = -\int_{-b_R}^{b_R} K_c(z-y) f_{k,s_i n_i}(r,y)\frac{dy}{b_R}, \tag{3.22}$$

that must be solved to determine $f_{k,s_i n_i}(r,z)$. From the derivation of the Kernel in this case, it is easily seen that to evaluate K_c for the rotor, the parameters above for the stator now must be changed to:

$$\beta_r: \quad \sqrt{1-M_{rR}^2},$$

Reduced frequency: $\quad K = -kV\Omega b_R/(\beta_r^2 c_R),$

Inter-blade gap: $\quad h = 2\pi r/B,$

Blade stagger angle: $\quad -\alpha_R,$

$$\Gamma: \quad +\frac{2\pi kV}{B}[1-M_T M_{rR}(r/r_D)\sin\alpha_R/\beta_r^2].$$

In the above, c_R is the nominal speed of sound in the rotor element region and M_{rR} is the Mach number of rotor relative flow, U_{rR}/c_R. The differences in Γ between the stator and rotor are due to the fact that for the stator the inter-vane phase angle is given by $\sigma_S = -2\pi sB/V$, while for the rotor, its analog, the inter-blade phase angle, has the form $\sigma_R = +2\pi kV/B$ (see Ref. 3 for discussion of inter-blade phase angles).

3.2 Source Vector Coefficients and Scattering Coefficients

To find source vector coefficients and scattering coefficients from the loading, we use the formulas for acoustic output wave pressure modal amplitudes and vorticity output wave *u/m* modal amplitudes. The formulas and their derivations are given in Appendices A and B. These results are obtained by adapting the approaches found in Refs. 1 and 6, respectively, to the situation here.

The source vector coefficients B_{Wskn} for acoustic output waves (W = 1, 2), as per the definition given in Section 2.2, are just the pressure modal amplitudes p_{Wskn} given by Eq. (A.24) when the input loading is from the rotor wake upwash. Similarly, the source vector coefficients B_{Wskn} for vorticity output waves (W = 3) are just the *u/m* modal amplitudes given by Eq. (B.12). Thus we have

$$B_{Wskn} = \begin{cases} \int_{r_H}^{r_D} C_{Wskn}(r) w_s(r) \int_{-b}^{b} f_s(r,z) D_{Wskn}(r,z) dz dr & \text{for } W = 1,2, \\ \sum_{l=1}^{L} \{C_{Wskn}(r_l) w_s(r_l) \int_{-b}^{b} f_s(r_l,z) D_{Wskn}(r_l,z) dz\} \Delta r_l & \text{for } W = 3, \end{cases} \tag{3.23}$$

where the subscript W, which was implicit in the last section, is now shown explicitly. In the above, $w_s(r)$ is given by Eq. (3.2); $C_{Wskn}(r)$ and $D_{Wskn}(r, z)$ by Eqs. (A.25) and (A.26) for W = 1, 2; and by Eqs. (B.13) and (B.14) for W = 3. The elemental vane chordwise loading function $f_s(r, z)$ is determined by Eq. (3.21). As discussed in Appendix B and illustrated in Fig. B.1, for the vorticity wave case, the annular duct is subdivided into L sub-annuli with widths $\Delta r_l = (r_l - r_{l-1})$, l = 1, $\cdots$, L. At this stage, the interface for output waves is at x^S, the axial location where the stator leading edge intersects the hub.

To obtain scattering coefficients for the stator, we apply Eqs. (A.24) and (B.12) as above, only now the loading is that provided by unit modal amplitude standard input waves with w_{sW_i,k_in_i} given either by Eq. (3.11) or (3.12) with $A_{W_isk_in_i} = 1$. We have used subscripts i to denote input modal indices; since the input and output harmonics must be the same, no i has been used with s. We can write

$$S_{WW_isk;sk_in_i} = \begin{cases} \int_{r_H}^{r_D} C_{Wskn}(r) \tilde{w}_{sW_i,k_in_i}(r) \int_{-b}^{b} f_{sW_i,k_in_i}(r,z) D_{Wskn}(r,z) dz dr & \text{for } W = 1,2, \\ \sum_{l=1}^{L} \{C_{Wskn}(r_l) \tilde{w}_{sW_i,k_in_i}(r_l) \int_{-b}^{b} f_{sW_i,k_in_i}(r_l,z) D_{Wskn}(r_l,z) dz\} \Delta r_l & \text{for } W = 3, \end{cases} \tag{3.24}$$

where $W_i = 1, 2, 3$. Also, $\tilde{w}_{sW_i,k_in_i}(r)$ is defined by Eq. (3.11) or (3.12), and $C_{Wskn}(r)$ and $D_{Wskn}(r, z)$ are the same as before.

Thus far, the source vector coefficients given above are for output interfaces located where the leading edge of the stator meets the hub, i.e. at x^S. The same is true regarding the input and output interfaces for scattering coefficients. Refer now to Fig. 3.1, which shows prior and new interface locations. For the stator alone case, we shift the interfaces so that downstream-going input waves originate from an interface at x^2 and upstream-going input waves from an interface located at the farthest downstream stator trailing edge coordinate with respect to radius, x^e. Downstream-going output waves originate at interface x^e and upstream-going output waves at x^2. More generally, we designate the new input and output interfaces, respectively, as x^{P_i} and x^P.

Because of the factor $e^{-i\gamma^P_{Wskn}(x_1 - x^P)}$ in Eqs. (2.1) and (2.6) for standard waves, it is easily seen that the modal amplitudes of output waves associated with source vector coefficients are changed by an amount

$$E^P_{Wskn} = e^{-i\gamma_{Wskn}(x^P - x^S)}, \tag{3.25}$$

where γ_{Wskn} is the axial wave number in the stator element region. Scattering coefficients are the ratios of the output to the input of state vector coefficients, i.e. $A^P_{Wskn} / A^{P_i}_{W_isk_in_i}$; therefore, using reasoning similar to that above, scattering coefficients must be multiplied by the ratio of the output to input shift exponentials, which is the ratio

$$F^{PP_i}_{WW_isk_n;sk_in_i} = \frac{e^{-i\gamma_{Wskn}(x^P - x^S)}}{e^{-i\gamma_{W_isk_in_i}(x^{P_i} - x^S)}}. \tag{3.26}$$

Thus Eqs. (3.23) and (3.24) become

$$B^P_{Wskn} = \begin{cases} E^P_{Wskn} \int_{r_H}^{r_D} C_{Wskn}(r) w_s(r) \int_{-b}^{b} f_s(r,z) D_{Wskn}(r,z) dz dr \quad for\ W = 1,2, \\ E^P_{Wskn} \sum_{l=1}^{L} \{C_{Wskn}(r_l) w_s(r_l) \int_{-b}^{b} f_s(r_l,z) D_{Wskn}(r_l,z) dz\} \Delta r_l \quad for\ W = 3, \end{cases} \tag{3.27}$$

and

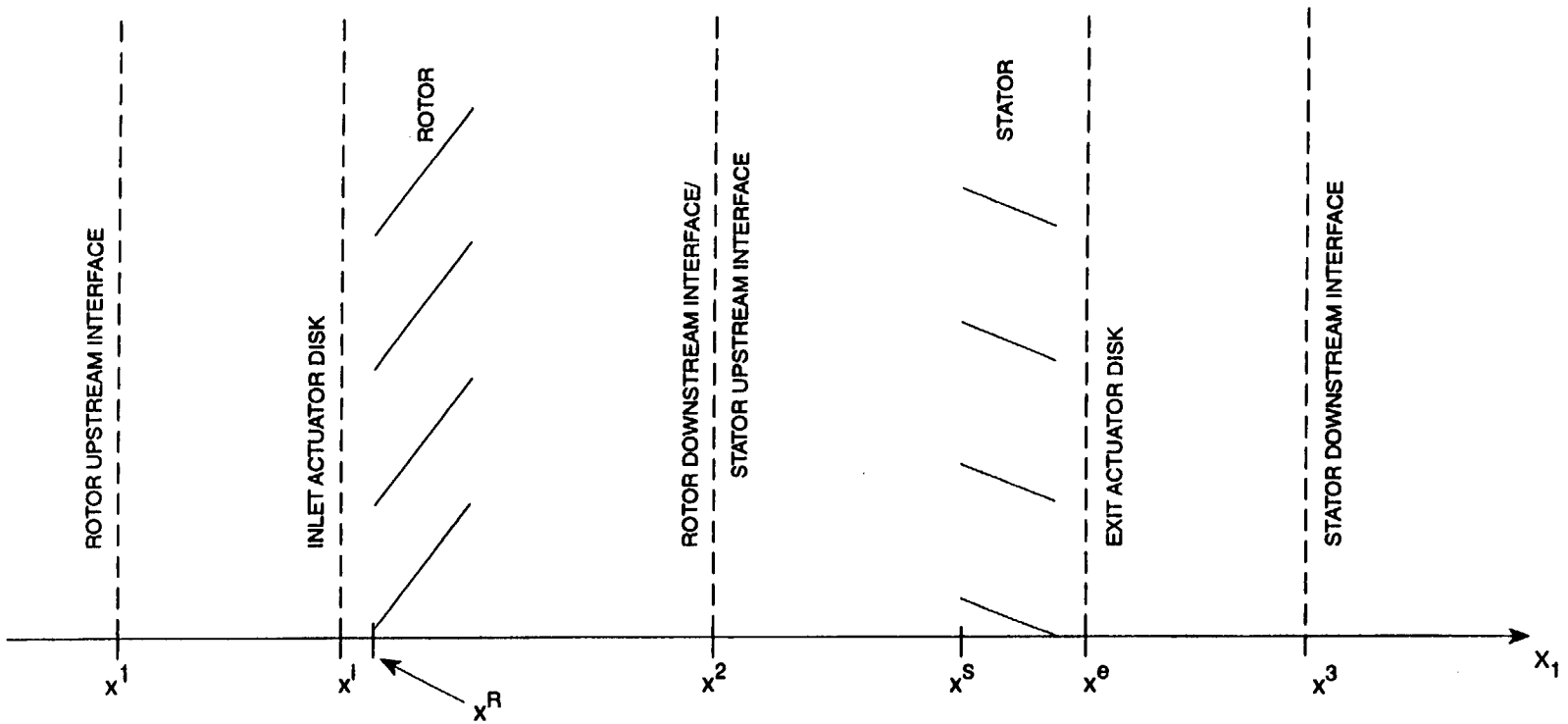

FIGURE 3.1 AXIAL INTERFACE COORDINATES AT THE HUB

$$S^{PP_i}_{WW_i skn;sk_in_i} = \begin{cases} F^{PP_i}_{WW_i skn;sk_in_i} \int_{r_H}^{r_D} C_{Wskn}(r)\tilde{w}_{sW_i,k_in_i}(r) \int_{-b}^{b} f_{sW_i,k_in_i}(r,z) D_{Wskn}(r,z)dzdr & \text{for } W = 1,2, \\ F^{PP_i}_{WW_i skn;sk_in_i} \sum_{l=1}^{L} \{C_{Wskn}(r_l)\tilde{w}_{sW_i,k_in_i}(r_l) \int_{-b}^{b} f_{sW_i,k_in_i}(r_l,z) D_{Wskn}(r_l,z)dz\}\Delta r_l & \text{for } W = 3, \end{cases}$$

(3.28)

where W_i = 1, 2, 3. For cut-on waves, the F's of Eq. (3.26) merely amount to a phase shift. However, for input or output waves that are cut off, the F's include real exponentials. These quantities serve the essential role of keeping reflection and transmission coefficients small for decaying waves and avoiding large off-diagonal elements in the scattering matrix.

Scattering coefficients for the rotor are derived analogously. Using Eqs. (A.45) and (B.15) of Appendices A and B, respectively, we have

$$S^{PP_i}_{WW_i skn;s_ikn_i} = \begin{cases} F^{PP_i}_{WW_i skn;s_ikn_i} \int_{r_H}^{r_D} C_{Wskn}(r)\tilde{w}_{kW_i,s_in_i}(r) \int_{-b_R}^{b_R} f_{kW_i,s_in_i}(r,z) D_{Wskn}(r,z)dzdr & \text{for } W = 1,2, \\ F^{PP_i}_{WW_i skn;s_ikn_i} \sum_{l=1}^{L} \{C_{Wskn}(r_l)\tilde{w}_{kW_i,s_in_i}(r_l) \int_{-b_R}^{b_R} f_{kW_i,s_in_i}(r_l,z) D_{Wskn}(r_l,z)dz\}\Delta r_l & \text{for } W = 3, \end{cases}$$

(3.29)

where W_i = 1, 2, 3. Additionally, $\tilde{w}_{kW_i,s_in_i}(r)$ is given by Eq. (3.18) or (3.19), and $C_{Wskn}(r)$ and $D_{Wskn}(r_l,z)$ by Eqs. (A.46) and (A.47) or Eqs. (B.16) and (B.17).

The term $F^{PP_i}_{WW_i skn;s_ikn_i}$ in Eq. (3.29) shifts the location of the input and output interfaces in analogous fashion to $F^{PP_i}_{WW_i skn;sk_in_i}$ for the stator case. It is given by

$$F^{PP_i}_{WW_i skn;s_ikn_i} = \frac{e^{-i\gamma_{Wskn}(x^P - x^R)}}{e^{-i\gamma_{W_is_ikn_i}(x^{P_i} - x^R)}}. \tag{3.30}$$

Without this factor, the interface for both input and output waves would be located where the rotor leading edge meets the hub, i.e. at x^R. Instead, referring to Fig. 3.1, the output interface is at x^2 for downstream-going waves and at x^i, the farthest upstream trailing edge location with respect to radius, for upstream-going waves. Input interfaces for upstream- and downstream-

going waves are the reverse. The variables x^{P_i} and x^P represent the locations x^2 and x^i, depending on the context, and γ_{Wskn} is the axial wave number in the rotor element region.

There is an additional item that must be taken care of before the standalone scattering coefficients are completely specified. For both the stator and rotor, we must add a term $1 \times F^{PP_i}_{WWskn;skn}$ to the transmission coefficients for those waves that are scattered into themselves, i.e. waves for which $W_i = W$, $s_i = s$, $k_i = k$, $n_i = n$. This term is added to account for transmission of the original wave through the stator or rotor. Though not appearing explicitly in Eqs. (3.28) and (3.29), this term will now be understood to be included where appropriate. The function $F^{PP_i}_{WWskn;skn}$ is defined either by Eq. (3.26) or (3.30), except that the subscript i is removed from all variables except P_i in those definitions.

Before closing, it should be noted that SOURCE3D employs non-dimensional geometry and performance parameters rather than the dimensional ones used above. This means that for the stator it utilizes lengths r_D and b_T and speeds c_S, U_S, and U_{rS}, defined with respect to the stator element region. Here, b_T is the vane semi-chord at the tip. Using these parameters, the formulas defining the stator source vector coefficients and scattering coefficients can be written in terms of the dimensionless variables $M_S = U_S/c_S$; $\sigma_{cS} = 2b_T/r_D$; $\sigma_r = r_H/r_D$; $\tilde{\gamma}_{skn} = \gamma_{skn} r_D$; $\tilde{k}_{skn} = k_{skn} r_D$; M_T, the rotor rotational Mach number at the blade tip; M_s, the swirl rotational Mach number at the blade tip; $X_{mn} = \kappa_{mn} r_D$; $x = r/r_D$; $x_S = x_{SD}/2b_T$; $y_S = y_{SD}/2b_T$; $x_{SOR} = x_{SPAC}/2b_T$; and $\tilde{b} = b/2b_T$. Non-dimensionalization is carried through in the rotor case using analogous rotor parameters and dimensionless variables.

CHAPTER 4

ADDITIONAL THEORY

Two additional items of theory will be needed to complete the calculation of source vector coefficients and scattering coefficients: a discussion of flow turning using an actuator disk, and then a discussion of a combined element to couple either the stator and actuator disk or the rotor and actuator disk into one element. These topics will be covered in the sections below.

4.1 Flow Turning at the Stator and Rotor

The theory developed thus far provides swirl between the rotor and stator, but does not include the flow turning at the rotor and stator that must accompany it. In this section, results will be presented that extend the two-dimensional approach of Ref. 3 to the three-dimensional situation shown in Fig. 4.1. A first disk will turn the flow at the rotor leading edge and a second one will straighten it back again at the stator trailing edge. The jumps in mean flow properties are given by input to the prediction program. Then the associated jumps in unsteady properties, such as pressure, axial velocity, and tangential velocity, are determined using linearized versions of the equations of conservation of mass, transverse momentum, and axial momentum.

With reference to Fig. 3.1, the actuator disks are located at the inlet interface x^i, which is the furthest upstream axial location with respect to radius of the rotor leading edge, and at the exit interface x^e, which is the furthest downstream axial location with respect to radius of the stator trailing edge. Input and output waves for the rotor actuator disk have their origins at the rotor upstream interface x^1 and at x^i. Input and output waves for the stator actuator disk originate at x^e and at the stator downstream interface x^3. Note that these locations are not the final ones for rotor and stator input and output waves. These locations will be set by the combined rotor and stator elements discussed in the next section.

Scattering coefficients at the actuator disks are based on the reflection and transmission of standard waves impinging on the disks. The harmonic indices s and k – and therefore m, stay the same for both input and output waves, so that actuator disk scattering is only among wave types (pressure and vorticity) and among radial mode orders. Similar to the two-dimensional situation (Ref. 3), there are three possible types of scattering. These interactions are shown in Fig. 4.2, where, for simplicity, only the subscript W, for W = 1, 2, 3, has been included with the state vector coefficient A; the indices P, s, k, and n_i or n are implied but not shown. The parameters A_1 and A_2 are pressure amplitudes, shown as solid arrows; the quantity A_3 represents the amplitude u/m for vorticity waves, shown as dashed arrows. In Fig. 4.2, incident pressure wave A_1 gives transmitted pressure wave A_1, reflected pressure wave A_2, and reflected vorticity wave A_3. Inputs A_2 and A_3 give similar results. Nine scattering coefficients will result from these interactions for each set of indices s, k, n_i, and n. The others will be zero.

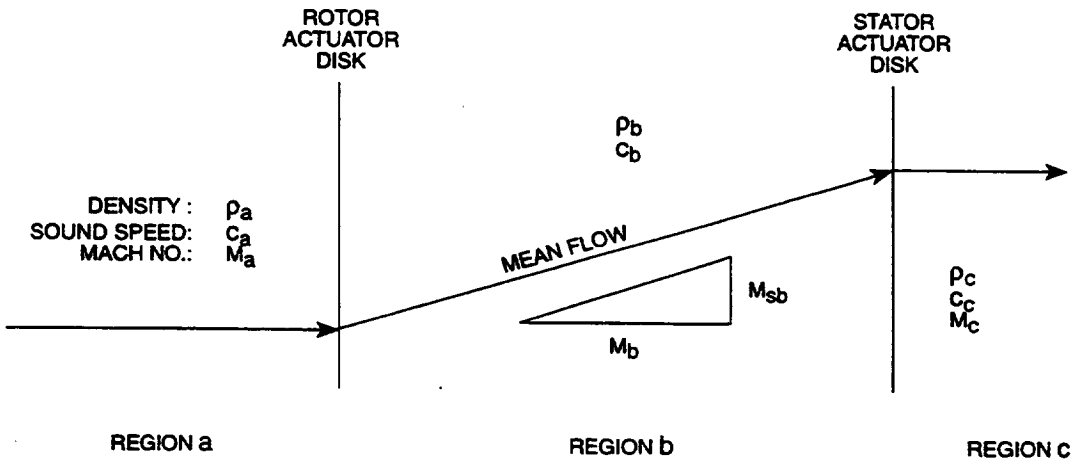

FIGURE 4.1 FLOW TURNING AT ROTOR AND STATOR

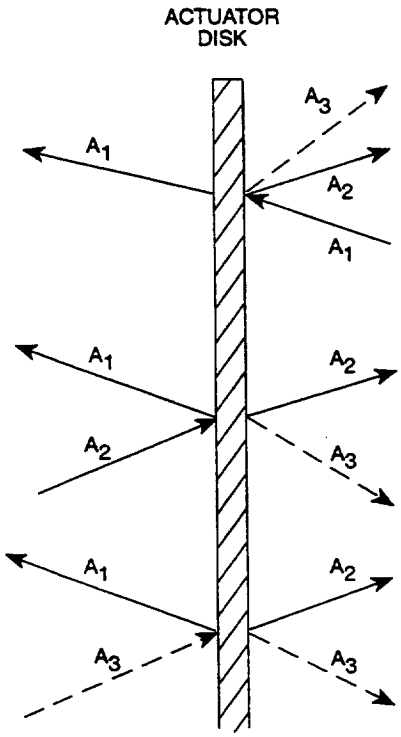

FIGURE 4.2 **THE THREE POSSIBLE TYPES OF SCATTERING INTERACTION (SOLID ARROWS REPRESENT PRESSURE WAVES, DASHED ARROWS VORTICITY WAVES. A_W, W=1,2,3, DENOTE STATE VECTOR AMPLITUDES.)**

Scattering coefficients will first be derived for input and output wave origins at the actuator disk axial locations. Later, the wave origins will be shifted to the desired locations shown in Fig. 3.1. The details of the derivation of these results are given in Appendix C. The results in this Appendix hold for both the rotor and stator; only the input data for each will be different. As discussed in Ref. 11, the actuator disk scattering coefficients are given by the elements of the matrix $\boldsymbol{K}_{io}$, derived there, and given by Eq. (C.58) here. This quantity satisfies the matrix equation

$$\boldsymbol{A}_{out} = \boldsymbol{K}_{io}\,\boldsymbol{A}_{in}, \tag{4.1}$$

where $\boldsymbol{A}_{in}$ and $\boldsymbol{A}_{out}$ are vectors made up, respectively, of input and output state vector coefficients. They are given by

$$\boldsymbol{A}_{in} = \begin{Bmatrix} A_1^b \\ A_2^a \\ A_3^a \end{Bmatrix}, \qquad \boldsymbol{A}_{out} = \begin{Bmatrix} A_1^a \\ A_2^b \\ A_3^b \end{Bmatrix}, \tag{4.2}$$

where the elements A_W^P in the brackets above are the vectors defined at the end of Section 2.2. The quantity a denotes values on the upstream side of the actuator disk, i.e. those before the jump; b represents values on the downstream side, i.e. those after the jump. The elements of $\boldsymbol{K}_{io}$ give the ratios $A_{Wskn}^{P} / A_{W_i skn_i}^{P_i}$.

To obtain the final actuator disk scattering coefficients, the input/output wave interfaces must be shifted to x^1 and x^i for the rotor disk, and to x^3 and x^e for the stator disk. This is done using the same approach as for the stator or rotor alone in Section 3.2, only now the just-mentioned axial locations are used. Thus each scattering coefficient given by $\boldsymbol{K}_{io}$ must be multiplied by a factor $F_{WW_i skn;skn_i}^{PP_i}$ given by

$$F_{WW_i skn;skn_i}^{PP_i} = \frac{e^{-i\gamma_{Wskn}^{P}(x^P - x^i)}}{e^{-i\gamma_{W_i skn_i}^{P_i}(x^{P_i} - x^i)}} \tag{4.3}$$

for the rotor disk, and by

$$F_{WW_i skn;skn_i}^{PP_i} = \frac{e^{-i\gamma_{Wskn}^{P}(x^P - x^e)}}{e^{-i\gamma_{W_i skn_i}^{P_i}(x^{P_i} - x^e)}} \tag{4.4}$$

for the stator disk, where x^P and x^{P_i} are the appropriate new input/output interface locations. Hence, the final actuator disk scattering coefficients are given by the relation

$$S^{PP_i}_{WW_i skn;skn_i} = F^{PP_i}_{WW_i skn;skn_i} K_{ioWW_i skn;skn_i}, \tag{4.5}$$

where the $K_{ioWW_i skn;skn_i}$ are the individual elements of $\boldsymbol{K}_{io}$.

As previously mentioned, before the coefficients above can be used in SOURCE3D, they must be non-dimensionalized. This is accomplished in the same way as discussed previously at the end of Section 3.2, using the same dimensionless variables as described there. The additional dimensionless variable $\tilde{\lambda}^P_{Wskn} = \lambda^P_{Wskn} / c_P$, is also needed, where λ^P_{Wskn} is defined in Appendix C and c_P is the medium nominal speed of sound in the appropriate region.

4.2 Combined Elements

Thus far we have derived source vector coefficients and scattering coefficients for separate stator alone and actuator disk elements. We have also obtained scattering coefficients for separate rotor alone and actuator disk elements. Let us refer to the coordinates in Fig. 3.1. In the former case, the axial interfaces are at x^2 and x^e for the stator, and at x^e and x^3 for the disk. In the latter case, they are at x^i and x^2 for the rotor, and at x^1 and x^i for the disk.

However, SOURCE3D combines the stator and actuator disk into one element and does the same for the rotor and actuator disk. The combined stator/actuator disk element has axial interfaces at x^2 and x^3; the combined rotor/actuator disk element has interfaces at x^1 and x^2. Source vector coefficients and scattering coefficients for the combined elements are derived and presented in Appendix D. For the stator case, they are the elements of the source vector $\boldsymbol{B}_{COMB}$ and the scattering matrix $\boldsymbol{S}_{COMB}$ given there, respectively, by Eqs. (D.19) and (D.18). For the rotor case, the scattering coefficients are the elements of the scattering matrix $\boldsymbol{S}_{COMB}$ described there for the rotor. As should be obvious, the elements of $\boldsymbol{B}_{COMB}$ and $\boldsymbol{S}_{COMB}$ for the stator depend on values of standalone stator coefficients and actuator disk coefficients. The same is true for $\boldsymbol{S}_{COMB}$ for the rotor.

CHAPTER 5

CONCLUDING REMARKS

This report has provided the analytical documentation for the SOURCE3D Rotor Wake/Stator Interaction Code. Source vector coefficients and scattering coefficients have been derived for the stator and rotor source elements, each in isolation, for use in the three-dimensional TFaNS (Theoretical Fan Noise Design/Prediction System). They have been obtained by extending the approach of the earlier V072 Rotor Wake/Stator Interaction Code.

The V072 code uses only the stator as its noise source. The SOURCE3D program has added a rotor element, swirl flow and vorticity waves, actuator disks for flow turning, and combined stator/actuator disk and rotor/actuator disk elements. When used in TFaNS, the rotor element will allow frequency scattering and reflections from the rotor, neither of which V072 provides. As mentioned previously, frequency scattering is the mechanism by which an original blade passing frequency (BPF) harmonic is scattered into other harmonics. The inclusion of the rotor element, swirl, and actuator disks accounts for mode trapping and amplification in TFaNS and explains features of experimental engine noise data not predicted by V072 (see Ref. 10). Mode trapping, as described earlier, is the phenomenon where the BPF mode grows between the stator and rotor blade rows through repeated reflections. This mode does not escape through the inlet or exit, but its energy is scattered into higher harmonics and is dispersed at two and three times BPF.

It should be noted that the SOURCE3D program has been verified thoroughly vs. Hanson's CUP2D two-dimensional coupled cascade noise prediction code using thin annulus test cases. Based on a modified advanced ducted propeller (ADP) geometry, the test model had 16 blades, 22 vanes, and was run at a corrected rotor speed of 9,600 rpm. Hub radius r_H was 8.15 inches and outer radius r_D was 8.164 inches, giving an annulus that was sufficiently narrow for the case to be considered two-dimensional. For this situation, the two-dimensional predictions of CUP2D matched the three-dimensional predictions of SOURCE3D very closely. Comparisons were made for source vector coefficients and scattering coefficients for the stator and the rotor with and without swirl, with and without actuator disks, and for the actuator disks and the combined elements each in isolation. In all instances, the results were nearly identical.

It should be pointed out that for two situations, SOURCE3D occasionally gives values of scattering coefficients which are unrealistically large. When this occurs, it is generally obvious to the user. The problems are caused by limitations in the original V072 model that carry over to SOURCE3D due either to two-dimensional load divergence or to duct resonance at three-dimensional cut on. Load divergence is a phenomenon that occurs in the two-dimensional unsteady aerodynamic theory when the normal distance between vanes or blades is half the free space acoustic wavelength at one or more radial locations. The problem at duct cut on arises from the factor k_{mns} in the denominator of the three-dimensional Green's function and in three-dimensional mode amplitude equations such as Eq. (A.14). This factor, defined in Eq. (A.10), goes to zero at three-dimensional cut on. In a fully consistent three-dimensional theory, this zero

limit would be matched by a load distribution that also goes to zero at cut on. However, in the present model, our loading is based on two-dimensional strip aerodynamics. The two-dimensional loading does approach zero, but at the two-dimensional cut-on frequency. Because two-dimensional and three-dimensional cut-on frequencies are markedly different, computed pressure harmonics diverge at duct resonance. More will be said about these items in Ref. 12, which discusses three-dimensional scattering physics results using SOURCE3D.

In conclusion, the SOURCE3D code adds the critical new ingredients of swirl, frequency scattering, and flow turning to the previous capability. This allows us to make predictions that are much more complete than before.

APPENDIX A

PRESSURE MODAL AMPLITUDES FOR A SYSTEM WITH SWIRL

To obtain pressure modal amplitudes for the case where there is swirl between the rotor and stator, we apply an approach very similar to that in Meyer and Envia (Ref. 1) for the case where there is no swirl. There are separate formulas for the stator and rotor cases. As stated in Section 2.1, swirl is taken to be of solid body type ($V = \Omega_s r$) for the three-dimensional case here. It is implemented by letting the stator rotate at angular speed $\Omega_1 = -\Omega_s$, the negative of the swirl angular speed, and the rotor at angular speed Ω_2 (see Fig. 2.3). The difference, $(\Omega_1 - \Omega_2)$, is equal to Ω, where Ω is the rotor angular speed. For both the stator and rotor, the analysis starts in the inertial system and ends, finally, in the stator-fixed coordinate system, which is where modal amplitudes must be evaluated.

For the stator case, we begin with the Green's function equation for unsteady pressure, as given by Eq. (41) of Ref. 13.* It is written as

$$p(\boldsymbol{x},t) = -\int_{-\infty}^{\infty}\int_{S} \boldsymbol{n}(\boldsymbol{y})\cdot\nabla G(\boldsymbol{x},\boldsymbol{y},t-\tau)\Delta p(\boldsymbol{y},\tau)\,dS(\boldsymbol{y})\,d\tau \tag{A.1}$$

in the inertial reference system. In this equation, $\boldsymbol{x}$ and $\boldsymbol{y}$ are, respectively, the field point and source point duct coordinates, $\boldsymbol{x} = (r,\bar{\phi},x_1)$ and $\boldsymbol{y} = (r',\bar{\phi}',y_1)$; S is the airfoil surface area; $\boldsymbol{n}$, the unit normal to this surface; Δp, the pressure loading on this surface; ∇, the gradient operator; and t and τ, the field and source point times. The axial coordinate origin is taken to be at the location where the stator leading edge meets the hub, i.e. at $x_1 = x^S$ (see Fig. 3.1). For simplicity, the indices P and W have been omitted. It should be clear from context what they should be. $G(\boldsymbol{x}, y, t - \tau)$ is the Green's function given by

$$G(\boldsymbol{x},\boldsymbol{y},t-\tau) = -\frac{1}{4\pi i}\sum_{m=-\infty}^{\infty}\sum_{n=1}^{\infty}\frac{\Psi_{mn}(r)\Psi_{mn}(r')}{\Gamma}e^{im(\bar{\phi}-\bar{\phi}')}\int_{-\infty}^{\infty}\frac{1}{k_{mn}(\omega)}e^{i[\gamma_{mn}(\omega)(y_1-x_1)-\omega(t-\tau)]}d\omega\,, \tag{A.2}$$

where

$$\gamma_{mn}(\omega) = \frac{M_S\omega}{\beta^2 c_S} + \frac{k_{mn}(\omega)}{\beta^2}\,\mathrm{sgn}(y_1 - x_1) \tag{A.3}$$

and

$$k_{mn}(\omega) = \sqrt{\left(\frac{\omega}{c_S}\right)^2 - \beta^2\kappa_{mn}^2}\,. \tag{A.4}$$

* This reference was the predecessor of Ref. 1 as documentation for V072.

Also, $\Gamma = (r_D^2 - r_H^2)$; ω is radian frequency; c_S is the speed of sound in the stator element region; M_S is the axial flow Mach number, U_S/c_S, where U_S is the uniform axial velocity in the stator element region; and $\beta = \sqrt{1 - M_S^2}$. The other parameters have been defined previously.

Let us shift the source point y to the stator-fixed frame using the transformation

$$\bar{\phi}' = \phi' + \Omega_2 \tau = \phi' - \Omega_s \tau , \tag{A.5}$$

where ϕ' is the source point polar coordinate in the stator-fixed frame (see Fig. A.1). Also, we write $\Delta p(y,\tau)$ in Fourier series as

$$\Delta p(y,\tau) = \sum_{s=-\infty}^{\infty} \Delta p_s(y) e^{-sB\Omega\tau} , \tag{A.6}$$

where y is taken to be on the vane mid-surfaces S_M, which have unit normals $\hat{n}(y)$. Then, combining Eqs. (A.1), (A.2), (A.5), and (A.6), while rearranging, we can write $p(x,t)$ as

$$\begin{aligned} p(x,t) = \sum_{s=-\infty}^{\infty} \sum_{m=-\infty}^{\infty} \sum_{n=1}^{\infty} \Psi_{mn}(r) e^{im\bar{\phi}} \int_{-\infty}^{\infty} \frac{1}{4\pi i \Gamma k_{mn}(\omega)} e^{-i\gamma_{mn}(\omega)x_1 - i\omega t} \\ \times \int_{S_M} \Psi_{mn}(r') \hat{n}(y) \cdot \nabla_y \left[e^{i(-m\phi' + \gamma_{mn}(\omega) y_1)} \right] \Delta p_s(y) \int_{-\infty}^{\infty} e^{i(\omega - sB\Omega + m\Omega_s)\tau} d\tau dS(y) d\omega, \end{aligned} \tag{A.7}$$

where ∇_y is the gradient taken with respect to the y coordinates.

Next we integrate over $d\tau$, then over $d\omega$, while recalling that $\int_{-\infty}^{\infty} e^{ix\tau} d\tau = 2\pi\delta(x)$, where $\delta(x)$ is the Dirac delta function. Then $\omega = sB\Omega - m\Omega_s$ and we have

$$\begin{aligned} p(x,t) = \sum_{s=-\infty}^{\infty} \sum_{m=-\infty}^{\infty} \sum_{n=1}^{\infty} \Psi_{mn}(r) e^{i(m\bar{\phi} - \gamma_{mns} x_1)} e^{-i(sB\Omega - m\Omega_s)t} \frac{1}{2i\Gamma k_{mns}} \\ \times \int_{S_M} \Psi_{mn}(r') \hat{n}(y) \cdot \nabla_y \left[e^{i(-m\phi' + \gamma_{mns} y_1)} \right] \Delta p_s(y) dS(y), \end{aligned} \tag{A.8}$$

where

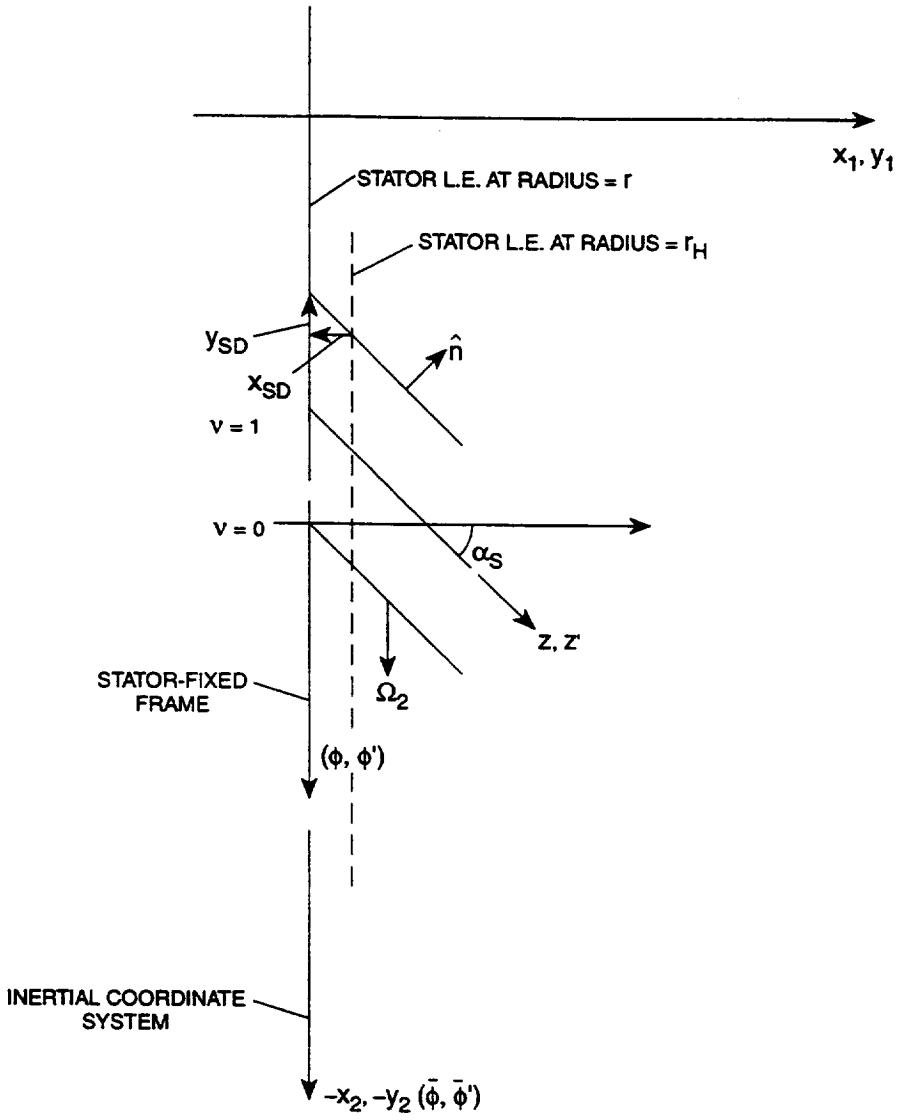

FIGURE A.1 STATOR GEOMETRY FOR ACOUSTIC WAVE MODAL ANALYSIS

$$\gamma_{mns} = \gamma_{mn}(sB\Omega - m\Omega_s)$$
$$= \frac{1}{\beta^2}\left[M_S\left(\frac{sB\Omega - m\Omega_s}{c_S}\right) \pm k_{mns}\right] \tag{A.9}$$

and

$$k_{mns} = k_{mn}(sB\Omega - m\Omega_s)$$
$$= \sqrt{\left(\frac{sB\Omega - m\Omega_s}{c_S}\right)^2 - \beta^2\kappa_{mn}^2}\,. \tag{A.10}$$

The (+)-sign in Eq. (A.9) is associated with upstream-going waves ($W = 1$) and the (-)-sign with downstream-going waves ($W = 2$).

Let us now shift the observer point y to the stator-fixed system where the modal coefficients are evaluated. We use the coordinate transformation

$$\bar{\phi} = \phi + \Omega_2 t = \phi - \Omega_s t\,, \tag{A.11}$$

where ϕ is the field point polar coordinate in the stator-fixed frame. Then Eq. (A.8) can be written as

$$p(\boldsymbol{x},t) = \sum_{s=-\infty}^{\infty}\sum_{m=-\infty}^{\infty}\sum_{n=1}^{\infty}\Psi_{mn}(r)e^{i(m\phi-\gamma_{mns}x_1)}e^{-isB\Omega t}\frac{1}{2i\Gamma k_{mns}}$$
$$\times\int_{S_M}\Psi_{mn}(r')\hat{\boldsymbol{n}}(\boldsymbol{y})\cdot\nabla_y\left[e^{i(-m\phi'+\gamma_{mns}y_1)}\right]\Delta p_s(\boldsymbol{y})dS(\boldsymbol{y}) \tag{A.12}$$

and $p(\boldsymbol{x}, t)$ has the form

$$p(\boldsymbol{x},t) = \sum_{s=-\infty}^{\infty}\sum_{m=-\infty}^{\infty}\sum_{n=1}^{\infty}p_{mns}\Psi_{mn}(r)e^{i(m\phi-\gamma_{mns}x_1-sB\Omega t)}\,, \tag{A.13}$$

In Eq. (A.13), p_{mns} is the modal amplitude coefficient we desire. It is given by

$$p_{mns} = \frac{1}{2i\Gamma k_{mns}}\int_{S_M}\Psi_{mn}(r')\hat{\boldsymbol{n}}(\boldsymbol{y})\cdot\nabla_y\left[e^{i(-m\phi'+\gamma_{mns}y_1)}\right]\Delta p_s(\boldsymbol{y})dS(\boldsymbol{y})\,. \tag{A.14}$$

This is the same as Eq. (4.29) of Ref. 1, except that now $(sB\Omega - m\Omega_s)$ has replaced $sB\Omega$ in the definitions of γ_{mns} and k_{mns}. The result of these transformations is that the axial wavenumber (and therefore cut-on frequency) given by Eqs. (A.9) and (A.10) has been modified

to a form exactly analogous to that of the two-dimensional theory. The procedure retains the correct frequencies, $sB\Omega$, in the stator frame.

From this point on, we proceed exactly as in Ref.1. Along with other relations, we use the expression

$$\hat{\boldsymbol{n}}(\mathbf{y})\cdot\nabla_{\mathbf{y}}\left[e^{i(-m\phi'+\gamma_{mns}y_1)}\right]=i\left(\frac{m}{r'}\cos\alpha_S+\gamma_{mns}\sin\alpha_S\right)e^{i(-m\phi'+\gamma_{mns}y_1)}, \tag{A.15}$$

the coordinate transformation

$$y_1=-x_{SD}+b\cos\alpha_S+z'\cos\alpha_S, \tag{A.16}$$

$$\phi'=(-y_{SD}+b\sin\alpha_S+z'\sin\alpha_S)/r', \tag{A.17}$$

and, the equality

$$\Delta p_s=\sum_{\nu=0}^{V-1}\rho_S U_{rS}w_s(r)f_s(r,z)e^{-2i\pi\nu sB/V}, \tag{A.18}$$

where ν is the vane index, $-2\pi sB/V$ is the inter-blade phase angle σ_S for the stator, z' is the source point chordwise coordinate along the vane, and the other parameters have been defined previously. For standard wave input, modal index subscripts are added to $w_s(r)$ and $f_s(r, z)$ in Chapter 3.

In this process, we also evaluate a summation

$$\sum_{\nu=0}^{V-1}e^{2\pi i\nu(m-sB)/V}, \tag{A.19}$$

which equals V when

$$m = sB - kV \tag{A.20}$$

and, otherwise, equals zero. The result is Eq. (4.36) of Ref. 1, which gives p_{mns} as

$$\begin{aligned}p_{mns}=\frac{\rho_S V}{2\Gamma k_{mns}}\int_{r_H}^{r_D}\Psi_{mn}(r)U_{rS}w_s(r)\left(\frac{m}{r}\cos\alpha_S+\gamma_{mns}\sin\alpha_S\right)\\ \times e^{i(-\gamma_{mns}x_{SD}+my_{SD}/r)}\int_{-b}^{b}f_s(r,z)e^{i[(\gamma_{mns}\cos\alpha_S-m\sin\alpha_S/r)(z+b)]}dzdr.\end{aligned} \tag{A.21}$$

Eq. (A.20) permits us to change the convention for the subscripts on p_{mns}, γ_{mns}, and k_{mns}, and to write Eq. (A.13) in the form

$$p_W(x,t) = \sum_{k=-\infty}^{\infty} \sum_{n=1}^{\infty} \sum_{s=-\infty}^{\infty} p_{Wskn} \Psi_{mn}(r) e^{i(m\phi - \gamma_{Wskn} x_1 - sB\Omega t)}, \tag{A.22}$$

where γ_{Wskn} and k_{Wskn} are given by the right-hand sides of Eqs. (A.9) and (A.10). Further, k_{mns} in Eq. (A.9) is now k_{Wskn} because W's have been made explicit. Additionally, $W = 1$ or 2, because output waves in this section are pressure waves. With this new notation, Eq. (A.21) can be written, finally, as

$$\begin{aligned} p_{Wskn} = \frac{\rho_S V}{2\Gamma k_{skn}} \int_{r_H}^{r_D} \Psi_{mn}(r) U_{rS} w_s(r) \left(\frac{m}{r} \cos\alpha_S + \gamma_{Wskn} \sin\alpha_S \right) \\ \times e^{i(-\gamma_{Wskn} x_{SD} + m y_{SD}/r)} \int_{-b}^{b} f_s(r,z) e^{i[(\gamma_{Wskn} \cos\alpha_S - m \sin\alpha_S / r)(z+b)]} dz dr. \end{aligned} \tag{A.23}$$

Note that this modal pressure amplitude is the same as that in Ref. 1, except for one major difference. Because of swirl, $(sB\Omega - m\Omega_s)$ has replaced $sB\Omega$ in γ_{Wskn} and k_{Wskn}. Further, observe that w_s and f_s will depend also on input wave modal indices k_i and n_i, in addition to s, for the case of standard wave input, as discussed in Chapter 3.

Eq. (A.23) can be written for later convenience as

$$p_{Wskn} = \int_{r_H}^{r_D} C_{Wskn}(r) w_s(r) \int_{-b}^{b} f_s(r,z) D_{Wskn}(r,z) dz dr, \tag{A.24}$$

where

$$C_{Wskn}(r) = \frac{\rho_S V U_{rS}}{2\Gamma k_{skn}} \Psi_{mn}(r) \left(\frac{m}{r} \cos\alpha_S + \gamma_{Wskn} \sin\alpha_S \right) e^{i(-\gamma_{Wskn} x_{SD} + m y_{SD}/r)}, \tag{A.25}$$

$$D_{Wskn}(r,z) = e^{i[(\gamma_{Wskn} \cos\alpha_S - m \sin\alpha_S / r)(z+b)]}. \tag{A.26}$$

For the rotor, we proceed similarly. Analogous to the stator case, the axial coordinate origin is taken at the point where the rotor leading edge meets the hub, i.e. at $x_1 = x^R$ (see Fig. 3.1). We start with Eq. (A.1) and shift $y = (r', \bar{\phi}', y_1)$ this time, however, from the inertial to the rotor-fixed frame. Here Eqs. (A.5) and (A.6) are replaced by

$$\bar{\phi}' = \hat{\phi}' + \Omega_1 \tau \tag{A.27}$$

and

$$\Delta p(y,\tau) = \sum_{k=-\infty}^{\infty} \Delta p_k(y) e^{-kV\Omega\tau}, \tag{A.28}$$

where $\hat{\phi}'$ is the source point polar coordinate in the rotor-fixed frame (see Fig. A.2).

Using these relations, the analog of Eq. (A.8) is

$$\begin{aligned} p(x,t) = \sum_{k=-\infty}^{\infty} \sum_{m=-\infty}^{\infty} \sum_{n=1}^{\infty} \Psi_{mn}(r) e^{i(m\bar{\phi} - \gamma_{mnk} x_1)} e^{-i(kV\Omega - m\Omega_1)t} \frac{1}{2i\Gamma k_{mnk}} \\ \times \int_{S_M} \Psi_{mn}(r') \hat{n}(y) \cdot \nabla_y \left[e^{i(-m\hat{\phi}' + \gamma_{mnk} y_1)} \right] \Delta p_k(y) dS(y), \end{aligned} \tag{A.29}$$

where S_M now represents the rotor blade mid-surfaces, and γ_{mnk} and k_{mnk} are given by Eqs. (A.3) and (A.4) with

$$\omega = kV\Omega + m\Omega_1. \tag{A.30}$$

Similar to before, we shift the field point x from the inertial to the stator-fixed coordinate system, using that

$$\bar{\phi} = \phi - \Omega_s t, \tag{A.31}$$

where ϕ is the field point polar coordinate in the stator-fixed system. Then the rotor counterpart of Eq. (A.13) becomes

$$p(x,t) = \sum_{k=-\infty}^{\infty} \sum_{m=-\infty}^{\infty} \sum_{n=1}^{\infty} p_{mnk} \Psi_{mn}(r) e^{i[m\phi - \gamma_{mnk} x_1 - (kV\Omega + m\Omega_1 + m\Omega_s)t]}, \tag{A.32}$$

where p_{mnk} is the modal amplitude for the $(kV\Omega + m\Omega_1 + m\Omega_s)^{\text{th}}$ harmonic. It is given by

$$p_{mnk} = \frac{1}{2i\Gamma k_{mnk}} \int_{S_M} \Psi_{mn}(r') \hat{n}(y) \cdot \nabla_y \left[e^{i(-m\hat{\phi}' + \gamma_{mnk} y_1)} \right] \Delta p_k(y) dS(y). \tag{A.33}$$

We will see later that Eq. (A.33) gives the modal amplitude we desire.

Eq. (A.33) is analogous to Eq. (A.14). Thus we proceed exactly as for the stator case, only in place of Eqs. (A.15)-(A.18), we use

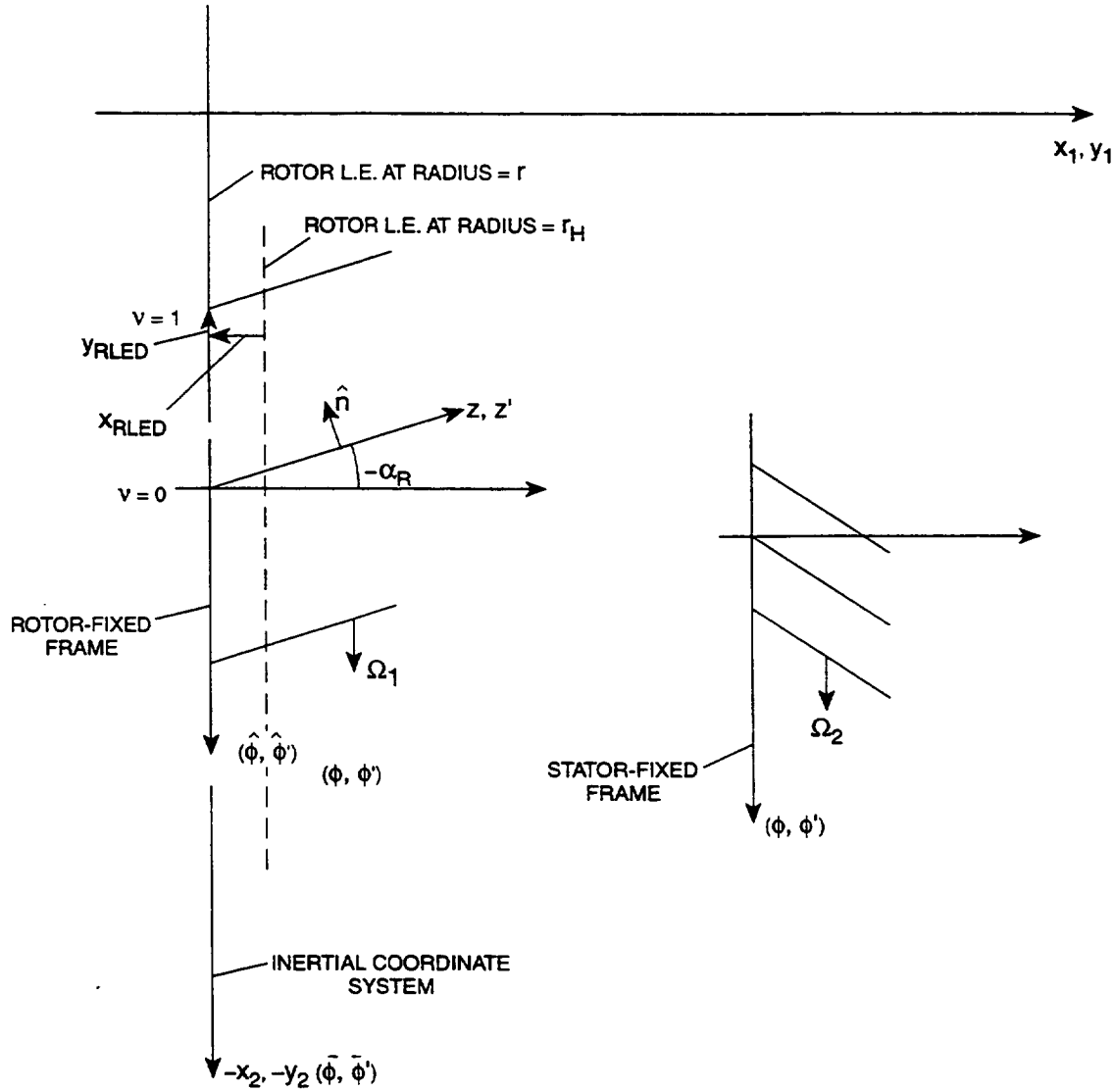

FIGURE A.2 ROTOR GEOMETRY FOR ACOUSTIC WAVE MODAL ANALYSIS

$$\hat{n}(y)\cdot\nabla_y\left[e^{i(-m\phi'+\gamma_{mnk}y_1)}\right]=i\left(\frac{m}{r'}\cos\alpha_R+\gamma_{mnk}\sin\alpha_R\right)e^{i(-m\hat{\phi}'+\gamma_{mnk}y_1)}, \tag{A.34}$$

$$y_1=-x_{RD}+b_R\cos\alpha_R+z'\cos\alpha_R, \tag{A.35}$$

$$\hat{\phi}'=(-y_{RD}+b_R\sin\alpha_R+z'\sin\alpha_R)/r', \tag{A.36}$$

$$\Delta p_k=\sum_{\nu=0}^{B-1}\rho_R U_{rR}w_k(r)f_k(r,z)e^{-2i\pi\nu kV/B}, \tag{A.37}$$

where z' is the source point chordwise coordinate along the blade. The exponent in Eq. (A.37) is different from that in Eq. (A.18) because the inter-blade phase angle σ_R for the rotor is $+2\pi kV/B$.* This procedure gives

$$\begin{aligned}p_{Wmnk}=&\frac{\rho_R B}{2\Gamma k_{mnk}}\int_{r_H}^{r_D}\psi_{mn}(r)U_{rR}w_k(r)\left(\frac{m}{r}\cos\alpha_R+\gamma_{Wmnk}\sin\alpha_R\right)\\&\times e^{i(-\gamma_{Wmnk}x_{RD}+my_{RD}/r)}\int_{-b_R}^{b_R}f_k(r,z)e^{i[(\gamma_{Wmnk}\cos\alpha_R-m\sin\alpha_R/r)(z+b_R)]}dzdr,\end{aligned} \tag{A.38}$$

where W's have been added.

In deriving Eq. (A.38), we evaluate a summation analogous to that in Eq. (A.19), i.e.,

$$\sum_{\nu=0}^{B-1}e^{2\pi i\nu(m+kV)/B}, \tag{A.39}$$

which equals B for

$$m = sB - kV \tag{A.40}$$

and is zero, otherwise. Hence m must assume the same values as it did for the stator.

Using Eq. (A.40) and the fact that $\Omega = \Omega_1 + \Omega_s$, we find that the time-dependent exponential in Eq. (A.32) can be rewritten as

$$\begin{aligned}e^{-i(kV\Omega+m\Omega_1+m\Omega_s)t}&=e^{-i(kV\Omega+m\Omega)t}\\&=e^{-i[kV\Omega+(sB-kV)\Omega]t}=e^{-isB\Omega t}.\end{aligned} \tag{A.41}$$

* The sign is the reverse of that for σ_S for the stator, because the relative motion between the rotor and stator is reversed.

Hence, we see that p_{Wmnk} is the modal amplitude we wish. Further, recalling Eq. (A.30), we have that

$$\begin{aligned}\omega &= kV\Omega + m\Omega_1 = kV\Omega + m(\Omega - \Omega_s \\ &= kV\Omega + (sB - kV)\Omega - m\Omega_s = sB\Omega - m\Omega_s,\end{aligned} \tag{A.42}$$

so ω is the same for the rotor as for the stator. Thus, referring to Eqs. (A.3) and (A.4), γ_{mnk} and k_{mnk} are the same as for the stator, i.e. they are given by Eqs (A.9) and (A.10), only M_S, c_S, and β there must be replaced by their rotor counterparts.

Changing the convention for the subscripts on p_{Wmnk}, γ_{Wmnk}, and k_{mnk}, as we did for the stator, we have, finally, that

$$p_W(x,t) = \sum_{k=-\infty}^{\infty} \sum_{n=1}^{\infty} \sum_{s=-\infty}^{\infty} p_{Wskn} \Psi_{mn}(r) e^{i(m\phi - \gamma_{Wskn} x_1 - sB\Omega t)} \tag{A.43}$$

and

$$\begin{aligned}p_{Wskn} = \frac{\rho_R B}{2\Gamma k_{skn}} \int_{r_H}^{r_D} \Psi_{mn}(r) U_{rR} w_k(r) \left(\frac{m}{r} \cos\alpha_R + \gamma_{Wskn} \sin\alpha_R \right) \\ \times e^{i(-\gamma_{Wskn} x_{RD} + m y_{RD}/r)} \int_{-b_R}^{b_R} f_k(r,z) e^{i[(\gamma_{Wskn} \cos\alpha_R - m \sin\alpha_R / r)(z + b_R)]} dz dr.\end{aligned} \tag{A.44}$$

In Chapter 3, subscripts s_i and n_i have been added to w_k and s_k to indicate that the upwash and associated loading are produced by input from standard waves that have these these modal indices. Similar to the case for the stator, p_{Wskn} can be rewritten as

$$p_{Wskn} = \int_{r_H}^{r_D} C_{Wskn}(r) w_k(r) \int_{-b}^{b} f_k(r,z) D_{Wskn}(r,z) dz dr, \tag{A.45}$$

where

$$C_{Wskn}(r) = \frac{\rho_R B U_{rR}}{2\Gamma k_{skn}} \Psi_{mn}(r) \left(\frac{m}{r} \cos\alpha_R + \gamma_{Wskn} \sin\alpha_R \right) e^{i(-\gamma_{Wskn} x_{RD} + m y_{RD}/r)}, \tag{A.46}$$

$$D_{Wskn}(r,z) = e^{i[(\gamma_{Wskn} \cos\alpha_R - m \sin\alpha_R / r)(z + b_R)]}. \tag{A.47}$$

APPENDIX B

VORTICITY WAVE MODAL AMPLITUDES

For the present version of SOURCE3D, we use a simplified two-dimensional/three-dimensional approach to compute the axial velocity modal amplitudes for the vorticity waves. This is done by placing "very thin" sub-annuli at each radius r of the duct (Fig. B.1a) and applying a two-dimensional Smith formula (Refs. 3 and 6) to the stator or rotor in each sub-annulus modeled as a two-dimensional cascade. This gives us the axial velocity at each r across the duct. We match these values radially, on an (s, k)-mode-by-mode basis, to values given by the three-dimensional expression for the vorticity wave axial velocity, which, at this point, has unknown modal coefficients. By doing this, we obtain an equation involving a Fourier series of the radial vorticity modal functions $U_n(r)$ from Chapter 2. This equation can be inverted to give the unknown modal coefficients, which are the vorticity modal amplitudes we set out to determine. In the course of this process we discretize the equations by dividing the annular duct into L sub-annuli (Fig. B.1b); each sub-annulus has radius r_l and thickness $\Delta r_l = (r_l - r_{l-1})$, $l = 1, \cdots, L$. The Smith formula approximations are calculated in each of these sub-annuli.

The two-dimensional axial velocity $u(x,t)$ associated with a vorticity wave at a single frequency ω for a two-dimensional cascade (Fig. B.2) can be deduced from S. N. Smith's report (Ref. 6) to be

$$u(x,t) = \int_0^c \frac{\Gamma(z_0)}{s} \sum_{k=-\infty}^{\infty} \tilde{u}_3 e^{i(\alpha_3 x + \beta y + \omega t)} e^{-i(\alpha_3 \cos\theta + \beta \sin\theta) z_0} dz_0 \qquad \text{(B.1)}$$

for the stator in the stator-fixed coordinate system. The notation is that of Ref. 3, where c is blade chord length; Γ, vortex strength representing loading; z_0, vane chord coordinate; s, vane spacing; $\tilde{u}_3$, a function given by Smith; α_3, axial wavenumber; β, transverse wavenumber; ω, angular frequency; and θ is stagger angle. The reader is referred to Ref. 3 for further details. For a sub-annulus of fixed radius r, treated as a two-dimensional cascade, Eq. (B.1) can be rewritten in our notation with all the harmonics of blade passing frequency as

$$u(\bar{x},t) = \sum_{k=-\infty}^{\infty} \sum_{s=-\infty}^{\infty} \bar{u}_{sk}(r) e^{i(m\bar{\phi} - \gamma_{sbn}\bar{x}_1 - sB\Omega t)}, \qquad \text{(B.2)}$$

where

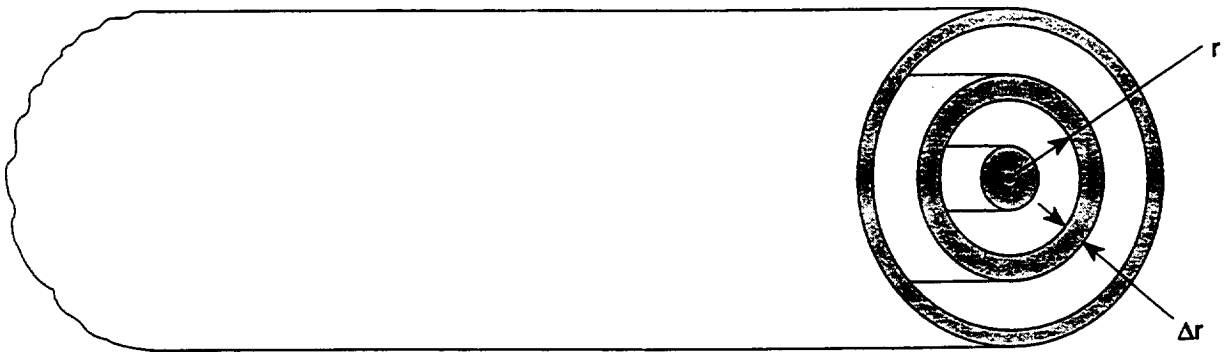

(A) DUCT WITH SUB-ANNULUS AT RADIUS = r

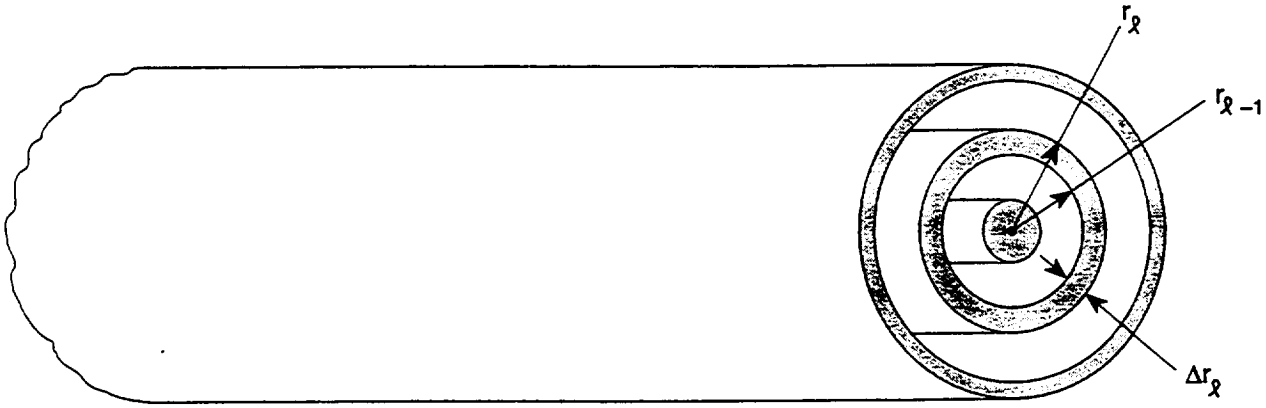

(B) SUBDIVIDED ANNULAR DUCT

FIGURE B.1 GEOMETRY FOR SUBDIVIDED ANNULAR DUCT

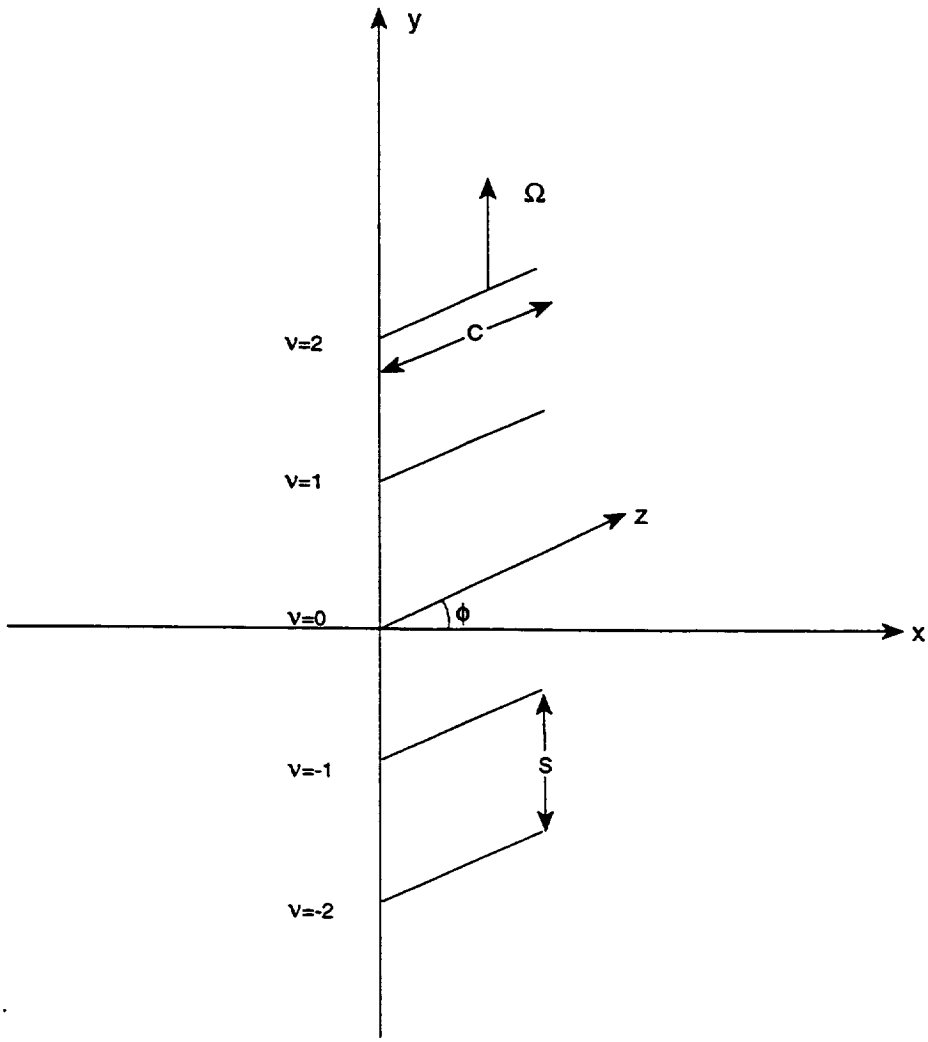

FIGURE B.2 TWO-DIMENSIONAL STATOR CASCADE

$$\bar{u}_{sk}(r) = -\frac{a_\infty V U_S m}{\pi r}\frac{w_s(r)}{U_{rS}}\frac{\left(\frac{sB\Omega r}{U_{rS}}\right)}{\left[\left(\frac{sB\Omega r}{U_{rS}}\right)^2 + m^2 - 2\left(\frac{sB\Omega r}{U_{rS}}\right)m\sin\alpha_S\right]} \times \int_{-b}^{b} f_s(r,z)e^{i[(\gamma_{skn}\cos\alpha_S - m\sin\alpha_S/r)(z+b)]}dz. \tag{B.3}$$

The coordinate system is that shown in the "unrolled" geometry of Fig. B.3, with $\bar{x}$ specified by the cylindrical polar coordinates $(r,\bar{\phi},\bar{x}_1)$. The axes are attached to the stator at the leading edge at each radius = r location. As before, m = sB - kV. Also, $\gamma_{skn} = (m\Omega_s - sB\Omega)/U_S$, by virtue of Eq. (2.8); other variables have been defined previously. As mentioned in Appendix A, w_s and f_s will have additional subscripts, k_i and n_i, for the case in Chapter 3, where the input is standard waves.

The three-dimensional axial velocity, $u(x, t)$, will have the same form as given in Chapter 2 for standard vorticity type waves. We write it as

$$u(x,t) = a_\infty \sum_{k=-\infty}^{\infty}\sum_{s=-\infty}^{\infty}\sum_{n=1}^{\infty}\left(\frac{u_{skn}}{m}\right)U_n(r)e^{i(m\phi - \gamma_{skn}x_1 - sB\Omega t)} \tag{B.4}$$

in the stator-fixed coordinate system. Here, x = (r, ϕ, x_1), where x_1 has its origin at the leading edge of the stator at the hub (see Fig. B.3), which is where output waves originate for stator results in this section. The coefficients (u_{skn}/m) are the modal amplitudes we wish to determine. The inclusion of m in these coefficients is required to eliminate division by 0 when m = 0 in some of the formulas below. Subscripts W, which are equal to 3 for this case, have been omitted, but are implied. They will be added later.

We rewrite Eq. (B.4) in terms of the coordinates for $\bar{x}$, by applying the tranformation,

$$x_1 = \bar{x}_1 - x_{SD}, \tag{B.5}$$

$$\phi = \bar{\phi} - \frac{y_{SD}}{r}, \tag{B.6}$$

to Eq. (B.4). These relations were obtained using Fig. B.3. Eq. (B.4) then gives

$$u(\bar{x},t) = \sum_{k=-\infty}^{\infty}\sum_{s=-\infty}^{\infty}\left\{\sum_{n=1}^{\infty}\left(\frac{u_{skn}}{m}\right)e^{i(-my_{SD}/r + \gamma_{skn}x_{SD})}U_n(r)\right\}e^{i(m\bar{\phi} - \gamma_{skn}\bar{x}_1 - sB\Omega t)}. \tag{B.7}$$

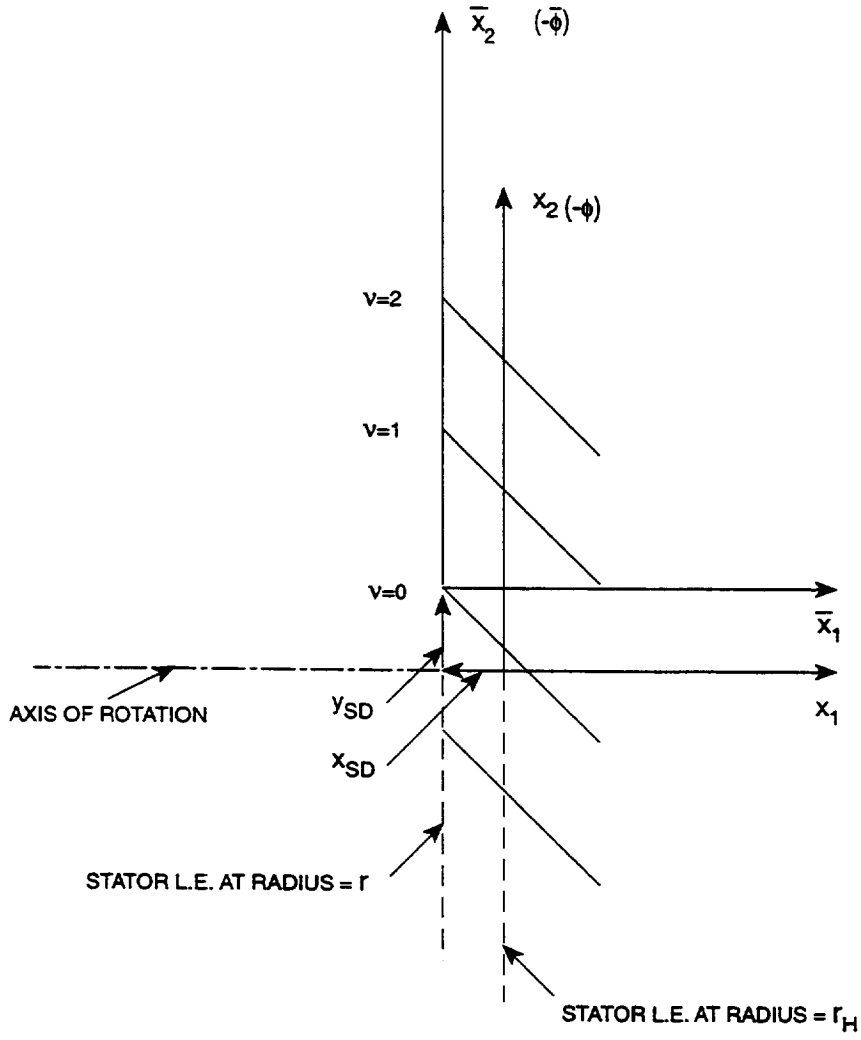

FIGURE B.3 STATOR GEOMETRY FOR VORTICITY WAVE MODAL ANALYSIS

To determine the coefficients (u_{skn}/m), we require the values of u specified by Eqs. (B.2) and (B.7) to match at each radius r. Because the exponential terms in these relations are the same, this means we must have

$$\bar{u}_{sk}(r) = \sum_{n=1}^{\infty} \left(\frac{u_{skn}}{m}\right) e^{i(-my_{SD}/r + \gamma_{skn} x_{SD})} U_n(r) \tag{B.8}$$

or, alternatively, that

$$\begin{aligned} \bar{u}_{sk}(r) e^{i(my_{SD}/r - \gamma_{skn} x_{SD})} &= \sum_{n=1}^{\infty} \left(\frac{u_{skn}}{m}\right) U_n(r) \\ &= \sum_{n=1}^{\infty} \left(\frac{u_{skn}}{m}\right) \cos\left[\frac{(n-1)\pi(r-r_H)}{r_D - r_H}\right], \end{aligned} \tag{B.9}$$

because the exponential in Eq. (B.8) is independent of n. The right-hand side is a Fourier series with coefficients (u_{skn}/m), so that, in essence, the two-dimensional r-dependent tranverse velocities have been resolved into radial modes.

Eq. (B.9) can be inverted and rearranged to give

$$\left(\frac{u_{skn}}{m}\right) = \frac{2}{r_D - r_D} \int_{r_H}^{r_D} \bar{u}_{sk}(r) e^{i(my_{SD}/r - \gamma_{skn} x_{SD})} U_n(r) dr\,. \tag{B.10}$$

In practice, $\bar{u}_{sk}(r)$ is evaluated only at the radii r_l, $l = 1, \cdots, L$, shown in Fig. B1b. Hence Eq. (B.10) must be rewritten in discrete form. It becomes

$$\left(\frac{u_{skn}}{m}\right) = \frac{2}{r_D - r_D} \sum_{l=1}^{L} \bar{u}_{sk}(r_l) e^{i(my_{SD}/r_l - \gamma_{skn} x_{SD})} U_n(r_l) \Delta r_l\,, \tag{B.11}$$

where $\Delta r_l = r_l - r_{l-1}$.

Finally, by recalling Eq. (B.3) and including W's, the above can be written more conveniently in the form

$$\left(\frac{u_{Wskn}}{m}\right) = \sum_{l=1}^{L} \left\{ C_{Wskn}(r_l) w_s(r_l) \int_{-b}^{b} f_s(r_l, z) D_{Wskn}(r_l, z) dz \right\} \Delta r_l\,, \tag{B.12}$$

where

$$C_{Wskn}(r_l) = -\frac{VU_S}{\pi(r_D - r_H)r_l}\frac{U_n(r_l)}{U_{rS}}\frac{\left(\frac{sB\Omega r_l}{U_{rS}}\right)}{\left[\left(\frac{sB\Omega r_l}{U_{rS}}\right)^2 + m^2 - 2\left(\frac{sB\Omega r_l}{U_{rS}}\right)m\sin\alpha_S\right]} e^{i(my_{SD}/r_l - \gamma_{Wskn}x_{SD})}, \quad \text{(B.13)}$$

$$D_{Wskn}(r_l, z) = e^{i[(\gamma_{Wskn}\cos\alpha_S - m\sin\alpha_S/r_l)(z+b)]}. \quad \text{(B.14)}$$

Because output waves in this section are vorticity waves, $W = 3$.

The modal amplitudes for the rotor are determined by a similar process. We make changes in Eq. (B.1) similar to those in going from stator to rotor in Ref. 3. We also change from $w_s(r_l)$ and $f_s(r_l, z)$ to $w_k(r_l)$ and $f_k(r_l, z)$, much as in Appendix A. In Chapter 3, subscripts s_i and n_i have been added to w_k and f_k, specifying the modal indices, because the input is from standard waves. Proceeding in parallel fashion to the stator case, we find that $u(x, t)$ is still given by Eq. (B.4), only now x_l has its origin where the leading edge of the rotor, rather than of the stator, meets the hub, so that output waves originate from this location. Further, Eqs. (B.12)-(B.14) are replaced by the relations

$$\left(\frac{u_{Wskn}}{m}\right) = \sum_{l=1}^{L}\left\{C_{Wskn}(r_l)w_k(r_l)\int_{-b_R}^{b_R} f_k(r_l, z)D_{Wskn}(r_l, z)dz\right\}\Delta r_l, \quad \text{(B.15)}$$

$$C_{Wskn}(r_l) = -\frac{BU_R}{\pi(r_D - r_H)r_l}\frac{U_n(r_l)}{U_{rR}}\frac{\left(\frac{kV\Omega r_l}{U_{rR}}\right)}{\left[\left(\frac{kV\Omega r_l}{U_{rR}}\right)^2 + m^2 - 2\left(\frac{kV\Omega r_l}{U_{rR}}\right)m\sin\alpha_R\right]} e^{i(my_{RD}/r_l - \gamma_{Wskn}x_{RD})}, \quad \text{(B.16)}$$

and

$$D_{Wskn}(r_l, z) = e^{i[(\gamma_{Wskn}\cos\alpha_R - m\sin\alpha_S/r_l)(z+b_R)]}, \quad \text{(B.17)}$$

so that Eq. (B.15) now gives the rotor modal amplitudes we desire.

APPENDIX C

SCATTERING COEFFICIENTS FOR ACTUATOR DISKS

This section extends the two-dimensional actuator disk theory of Ref. 3 to three dimensions. The extension here was first developed in private notes by D. B. Hanson and then developed further by the present author. As discussed in Chapter 4, there are two actuator disks. The first is at the leading edge of the rotor where it turns the mean axial flow to add swirl between the rotor and stator. The second is at the trailing edge of the stator where it returns the flow to the axial direction (see Fig. 4.1). The theory here applies to either of the two disks. The configuration used is shown in Fig. C.1. For simplicity, the actuator disk is located axially at $x_1 = 0$, which is where input and output waves also have their origins. The procedure for shifting the input and output wave interfaces is discussed in Section 4.1. Region *a* in Fig. C.1 will refer to the region on the upstream side of the actuator disk, region *b* to that on the downstream side.

We will derive scattering coefficients for the three types of wave interactions shown in Fig. 4.2 and discussed in Section 4.1. To do this, we will use the jump conditions provided by satisfying linearized mass, axial momentum, and transverse momentum conservation requirements across the disks. We do not include the effect of a radial component *w*. Radial equations are easily derived but are not part of the current formulation. The technique used is to write the flow variables as the sum of a mean part and a perturbation part (assumed to be small). Expressions for the conserved quantities on each side of a disk are equated. Mean flow quantities are determined and specified from a separate analysis. Jumps in the mean quantities at the disk necessitate jumps in the perturbation quantities according to the analysis of this section. The conservation requirements will be applied one (*s*, *k*)-mode at a time; harmonic indices *s* and *k* (and therefore *m*) will be fixed across the disk, because scattering occurs only on radial indices *n* and wave type. First, though, we will need formulas for all the acoustic wave and vorticity wave unsteady velocity components in terms of state vector amplitudes.

Velocity Components

Acoustic pressure can be written in standard wave form (see Eq. 2.1) as

$$p'^{P}_{W}(x_1, r, \phi, t) = p_\infty \sum_{s=-\infty}^{\infty} \sum_{k=-\infty}^{\infty} \sum_{n=1}^{\infty} A^{P}_{Wskn} \Psi_{mn}(r) e^{i(m\phi - \gamma^{P}_{Wskn} x_1 - sB\Omega t)}, \qquad \text{(C.1)}$$

where *P* will refer to either region *a* or *b*, and *W* will equal either 1 or 2. Superscript *P* is not needed here for $\Psi_{mn}(r)$, nor in the case later for $U_n(r)$, so it is omitted from these quantities.

We seek expressions for the associated axial and tranverse velocities in terms of the parameters A^{P}_{Wskn}. We write these velocities in the form

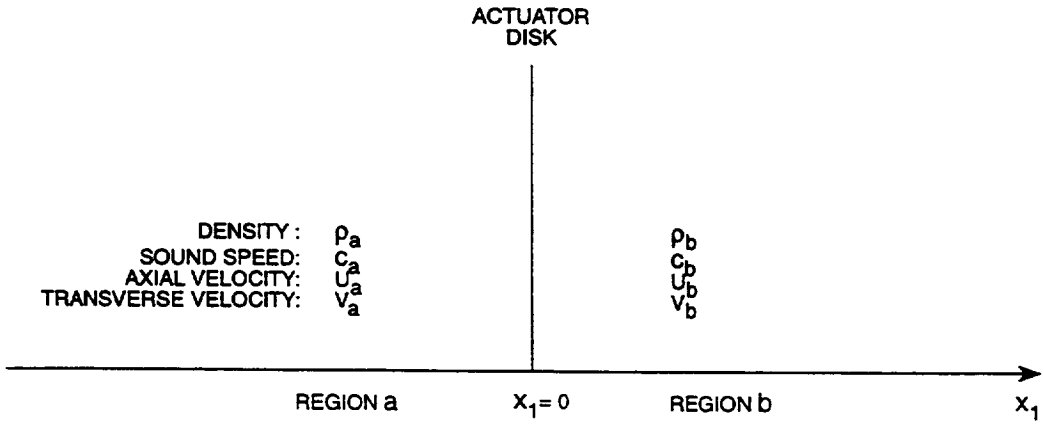

FIGURE C.1 CONFIGURATION FOR THE ACTUATOR DISK

$$u_W^P(x_1,r,\phi,t) = a_\infty \sum_{s=-\infty}^{\infty} \sum_{k=-\infty}^{\infty} \sum_{n=1}^{\infty} u_{Wskn}^P A_{Wskn}^P \Psi_{mn}(r) e^{i(m\phi - \gamma_{Wskn}^P x_1 - sB\Omega t)}, \tag{C.2}$$

$$v_W^P(x_1,r,\phi,t) = a_\infty \sum_{s=-\infty}^{\infty} \sum_{k=-\infty}^{\infty} \sum_{n=1}^{\infty} v_{Wskn}^P A_{Wskn}^P \Psi_{mn}(r) e^{i(m\phi - \gamma_{Wskn}^P x_1 - sB\Omega t)}, \tag{C.3}$$

and determine the unknown coefficients, u_{Wskn}^P and v_{Wskn}^P, through use of the momentum equation

$$\frac{\partial \boldsymbol{u}}{\partial t} + \boldsymbol{U} \cdot \nabla \boldsymbol{u} = -\frac{1}{\rho_0} \nabla p, \tag{C.4}$$

where $\boldsymbol{u} = (u, v, w)$ is the perturbation velocity; $\boldsymbol{U} = (U, V, 0)$, the mean velocity; ρ_0, the nominal fluid density; and p, the acoustic pressure.

Eq. (C.4) can be written as

$$\frac{\partial \boldsymbol{u}}{\partial t} + (U\frac{\partial}{\partial x_1} + \Omega_s \frac{\partial}{\partial \phi})\boldsymbol{u} = -\frac{1}{\rho_0} \nabla p, \tag{C.5}$$

if we recall that $\frac{\partial}{\partial x_2} = -\frac{1}{r}\frac{\partial}{\partial \phi}$. The (-)-sign in the preceding relation is a result of the fact that x_2 and ϕ are positive in opposite directions (Fig. 2.3). We have also used $V = -\Omega_s r$. Eq. (C.5) gives the axial momentum equation

$$\frac{\partial u}{\partial t} + U\frac{\partial u}{\partial x_1} + \Omega_s \frac{\partial u}{\partial \phi} = -\frac{1}{\rho_0}\frac{\partial p}{\partial x_1} \tag{C.6}$$

and the transverse momentum equation

$$\frac{\partial v}{\partial t} + U\frac{\partial v}{\partial x_1} + \Omega_s \frac{\partial v}{\partial \phi} = \frac{1}{\rho_0}\frac{1}{r}\frac{\partial p}{\partial \phi}. \tag{C.7}$$

If we substitute Eqs. (C.1) and (C.2) into Eq. (C.6) on a mode-by-mode basis, while replacing U and ρ_0 with U_P and ρ_P, we find that

$$u_{Wskn}^P = \frac{p_\infty}{a_\infty \rho_P} \frac{\gamma_{Wskn}^P}{\lambda_{Wskn}^P}, \tag{C.8}$$

where

$$\lambda_{Wskn}^P = -sB\Omega - U_P \gamma_{Wskn}^P + m\Omega_s. \tag{C.9}$$

Similarly, using Eqs. (C.1) and (C.3) in Eq. (C.7), we see that

$$v^P_{Wskn} = \frac{p_\infty}{a_\infty \rho_P r} \frac{m}{\lambda^P_{Wskn}}. \tag{C.10}$$

Thus we have

$$u^P_W(x_1,r,\phi,t) = p_\infty \sum_{s=-\infty}^{\infty} \sum_{k=-\infty}^{\infty} \sum_{n=1}^{\infty} \frac{\gamma^P_{Wskn}}{\rho_P \lambda^P_{Wskn}} A^P_{Wskn} \Psi_{mn}(r) e^{i(m\phi - \gamma^P_{Wskn} x_1 - sB\Omega t)} \tag{C.11}$$

and

$$v^P_W(x_1,r,\phi,t) = p_\infty \sum_{s=-\infty}^{\infty} \sum_{k=-\infty}^{\infty} \sum_{n=1}^{\infty} \frac{m}{\rho_P \lambda^P_{Wskn} r} A^P_{Wskn} \Psi_{mn}(r) e^{i(m\phi - \gamma^P_{Wskn} x_1 - sB\Omega t)}. \tag{C.12}$$

To obtain comparable results for vorticity waves, we write the axial velocity in standard wave form [see Eq. (2.6)] as

$$u^P_W(x_1,r,\phi,t) = a_\infty \sum_{s=-\infty}^{\infty} \sum_{k=-\infty}^{\infty} \sum_{n=1}^{\infty} m A^P_{Wskn} U_n(r) e^{i(m\phi - \gamma^P_{Wskn} x_1 - sB\Omega t)}, \tag{C.13}$$

where W now is 3.

We seek an expression for the transverse velocity in terms of the state vector coefficients A^P_{Wskn}. To do this, we write the transverse velocity as

$$v^P_W(x_1,r,\phi,t) = a_\infty \sum_{s=-\infty}^{\infty} \sum_{k=-\infty}^{\infty} \sum_{n=1}^{\infty} v^P_{Wskn} A^P_{Wskn} U_n(r) e^{i(m\phi - \gamma^P_{Wskn} x_1 - sB\Omega t)}. \tag{C.14}$$

and find v^P_{Wskn} through use of the continuity equation

$$\nabla \cdot \boldsymbol{u} = 0, \tag{C.15}$$

which must be satisfied by vorticity wave velocity components. This gives

$$\frac{\partial u}{\partial x_1} = -\frac{1}{r}\frac{\partial v}{\partial \phi}, \tag{C.16}$$

since the radial component for this wave type is zero. Substituting Eqs. (C.13) and (C.14) mode-by-mode into Eq. (C.16), we then have

$$\nu^{P}_{Wskn} = r\gamma^{P}_{Wskn}. \tag{C.17}$$

Thus we can rewrite Eq. (C.14) as

$$v^{P}_{W}(x_1, r, \phi, t) = a_\infty \sum_{s=-\infty}^{\infty} \sum_{k=-\infty}^{\infty} \sum_{n=1}^{\infty} r\gamma^{P}_{Wskn} A^{P}_{Wskn} U_n(r) e^{i(m\phi - \gamma^{P}_{Wskn} x_1 - sB\Omega t)}. \tag{C.18}$$

Conservation of Mass

As shown in Ref. 14, the first-order equation for conservation of mass can be written as

$$\rho_a \tilde{u}_a + \frac{U_a}{c_a^2} \tilde{p}_a = \rho_b \tilde{u}_b + \frac{U_b}{c_b^2} \tilde{p}_b, \tag{C.19}$$

where a and b are the same as before; the mean flow parameters ρ_a, ρ_b, U_a, U_b, are considered known; and items with tildas represent disturbance, i.e. fluctuating components. Eq. (C.19) is applied at the interface between regions a and b, where $x_1 = 0$.

Let us define

$$C_a = \frac{a_\infty}{p_\infty} (\rho_a \tilde{u}_a + \frac{U_a}{c_a^2} \tilde{p}_a), \tag{C.20}$$

$$C_b = \frac{a_\infty}{p_\infty} (\rho_b \tilde{u}_b + \frac{U_b}{c_b^2} \tilde{p}_b), \tag{C.21}$$

where $\frac{a_\infty}{p_\infty}$ is used for non-dimensionalization. Substituting values for $\tilde{p}_a$ and $\tilde{u}_a$ using Eqs. (C.1), (C.11), and (C.13), we have

$$C_a = \frac{a_\infty}{b_\infty} [\rho_a \sum_{n'=1}^{\infty} \frac{p_\infty}{\rho_a} \frac{\gamma^{a}_{1skn'}}{\lambda^{a}_{1skn'}} A^{a}_{1skn'} \Psi_{mn'}(r) + \frac{M_a}{c_a} p_\infty \sum_{n'=1}^{\infty} A^{a}_{1skn'} \Psi_{mn'}(r) +$$
$$\rho_a \sum_{n'=1}^{\infty} \frac{p_\infty}{\rho_a} \frac{\gamma^{a}_{2skn'}}{\lambda^{a}_{2skn'}} A^{a}_{2skn'} \Psi_{mn'}(r) + \frac{M_a}{c_a} p_\infty \sum_{n'=1}^{\infty} A^{a}_{2skn'} \Psi_{mn'}(r) + \rho_a a_\infty \sum_{n'=1}^{\infty} m A^{a}_{3skn'} U_{n'}(r)], \tag{C.22}$$

for each fixed set of indices (s, k). The radial index n' is used here to differentiate between this index and a second radial index n, which will be introduced later.* The factor $e^{i(m\phi - sB\Omega t)}$, which is part of the disturbance components, is omitted from Eq. (C.22), but implied.

* Note that, in the code, we have used the notation n_i rather than n'.

We approximate C_a, using finite sums, and write it more compactly as

$$C_a = \sum_{n'=1}^{N_1} \overline{C}^a_{1skn'} \psi_{mn'}(r) A^a_{1skn'} + \sum_{n'=1}^{N_2} \overline{C}^a_{2skn'} \psi_{mn'}(r) A^a_{2skn'} + \sum_{n'=1}^{N_3} \overline{C}^a_{3skn'} U_{n'}(r) A^a_{3skn'}, \qquad \text{(C.23)}$$

where, after simplification, we have

$$\overline{C}^a_{1skn'} = \frac{a_\infty \gamma^a_{1skn'}}{\lambda^a_{1skn'}} + \frac{a_\infty M_a}{c_a}, \qquad \text{(C.24)}$$

$$\overline{C}^a_{2skn'} = \frac{a_\infty \gamma^a_{2skn'}}{\lambda^a_{2skn'}} + \frac{a_\infty M_a}{c_a}, \qquad \text{(C.25)}$$

$$\begin{aligned} \overline{C}^a_{3skn'} &= \frac{a^2_\infty \rho_a m}{p_\infty} \\ &= 1.4 \left(\frac{p_a}{p_\infty} \right) \left(\frac{a_\infty}{c_a} \right)^2 m. \end{aligned} \qquad \text{(C.26)}$$

In going from the first to the second line in Eq. (C.26), we have used the relationship

$$\rho = 1.4 p / c^2 \qquad \text{(C.27)}$$

for isentropic flow of air. There exist relations analogous to Eqs. (C.23)-(C.26) for C_b, $\overline{C}^b_{1skn'}$, $\overline{C}^b_{2skn'}$, and $\overline{C}^b_{3skn'}$.

From a practical standpoint, we cannot satisfy Eq. (C.19) at all r, so instead we satisfy it in a Galerkin sense. We set $C_a = C_b$, multiply by $\frac{1}{g_{1n}} \psi_{mn}(r) r$, and integrate over dr from r_H to r_D, where

$$g_{1n} = \int_{r_H}^{r_D} \psi^2_{mn}(r) r dr. \qquad \text{(C.28)}$$

We do this for each n, $n = 1, \cdots, N_1$, to obtain the set of equations,

$$\sum_{n'=1}^{N_1} C^a_{1sknn'} A^a_{1skn'} - \sum_{n'=1}^{N_2} C^b_{2sknn'} A^b_{2skn'} - \sum_{n'=1}^{N_3} C^b_{3sknn'} A^b_{3skn'}$$

$$= \sum_{n'=1}^{N_1} C^b_{1sknn'} A^b_{1skn'} - \sum_{n'=1}^{N_2} C^a_{2sknn'} A^a_{2skn'} - \sum_{n'=1}^{N_3} C^a_{3sknn'} A^a_{3skn'}, \qquad (C.29)$$

$$n = 1, \cdots, N_1.$$

In writing this expression, we have placed the input A's, as shown in Fig. 4.2, on the right and the output ones on the left. The parameter g_{1n} in Eq. (C.28), and subsequent g's, will normalize diagonal elements to 1 in matrices that will be defined later. In Eq. (C.29),

$$C^P_{1sknn'} = \delta_{n,n'} \overline{C}^P_{1skn'}, \qquad (C.30)$$

$$C^P_{2sknn'} = \delta_{n,n'} \overline{C}^P_{2skn'}, \qquad (C.31)$$

$$C^P_{3sknn'} = \delta_{1n,n'} \overline{C}^P_{3skn'} \qquad (C.32)$$

for P = a or b. Further, $\delta_{n,n'}$ is the Kronecker delta (1 when n = n', 0 otherwise), and

$$\delta_{1n,n'} = \frac{1}{g_{1n}} \int_{r_H}^{r_D} U_{n'}(r) \psi_{mn}(r) r dr. \qquad (C.33)$$

Eq. (C.29) will be used later when we set up an overall matrix equation.

Conservation of Axial Momentum

The first-order unsteady axial momentum equation at the actuator disk is given by

$$(1 + M_a^2)\tilde{p}_a + 2\rho_a U_a \tilde{u}_a = (1 + M_b^2)\tilde{p}_b + 2\rho_b U_b \tilde{u}_b \qquad (C.34)$$

(see Ref. 14). Thus we require that

$$F_a = F_b, \qquad (C.35)$$

where

$$F_a = \frac{1}{p_\infty}[(1 + M_a^2)\tilde{p}_a + 2\rho_a U_a \tilde{u}_a], \qquad (C.36)$$

and F_b is the same, only with b's in place of a's. The factor $1/p_\infty$ is used for normalization.

Substituting standard wave expressions into F_a and F_b, truncating the sums as in Eq. (C.23), multiplying Eq. (C.35) by $\frac{1}{g_{1n}}\psi_{mn}(r)r$ for each $n = 1, \cdots, N_2$, and proceeding similarly to the conservation of mass case, we obtain the set of equations,

$$\sum_{n'=1}^{N_1} F^a_{1sknn'} A^a_{1skn'} - \sum_{n'=1}^{N_2} F^b_{2sknn'} A^b_{2skn'} - \sum_{n'=1}^{N_3} F^b_{3sknn'} A^b_{3skn'}$$
$$= \sum_{n'=1}^{N_1} F^b_{1sknn'} A^b_{1skn'} - \sum_{n'=1}^{N_2} F^a_{2sknn'} A^a_{2skn'} - \sum_{n'=1}^{N_3} F^a_{3sknn'} A^a_{3skn'}, \qquad (C.37)$$
$$n = 1, \cdots, N_2.$$

This is the second set of equations needed for the final matrix equation. In Eq. (C.37),

$$F^P_{1sknn'} = \delta_{n,n'}[(1+M_P^2) + 2c_P M_P \frac{\gamma^P_{1skn'}}{\lambda^P_{1skn'}}], \qquad (C.38)$$

$$F^P_{2sknn'} = \delta_{n,n'}[(1+M_P^2) + 2c_P M_P \frac{\gamma^P_{2skn'}}{\lambda^P_{2skn'}}], \qquad (C.39)$$

$$F^P_{3sknn'} = \delta_{1n,n'}[2(1.4)M_P\left(\frac{p_P}{p_\infty}\right)\left(\frac{a_\infty}{c_P}\right)m] \qquad (C.40)$$

for $P = a$ or b.

Conservation of Transverse Momentum

The first-order unsteady transverse momentum equation is derived by retaining only the first-order terms from Eq. (D-23) of Ref. 14. It is given by

$$\rho_a U_a \tilde{v}_a + \rho_a V_a \tilde{u}_a + \tilde{\rho}_a U_a V_a = \rho_b U_b \tilde{v}_b + \rho_b V_b \tilde{u}_b + \tilde{\rho}_b U_b V_b. \qquad (C.41)$$

Since $p = \rho c^2$, $V_a = \Omega_{sa} r$, and $V_b = \Omega_{sb} r$, where Ω_{sa} and Ω_{sb} are swirl angular velocities in regions a and b, this can be written as

$$\rho_a U_a \tilde{v}_a + \rho_a \Omega_{sa} r \tilde{u}_a + M_a\left(\frac{\Omega_{sa} r}{c_a}\right)\tilde{p}_a = \rho_b U_b \tilde{v}_b + \rho_b \Omega_{sb} r \tilde{u}_b + M_b\left(\frac{\Omega_{sb} r}{c_b}\right)\tilde{p}_b. \qquad (C.42)$$

Let us set

$$G_a = \frac{1}{p_\infty}\left[\rho_a U_a \tilde{v}_a + \rho_a \Omega_{sa} r \tilde{u}_a + M_a\left(\frac{\Omega_{sa} r}{c_a}\right)\tilde{p}_a\right] \qquad (C.43)$$

and define G_b analogously. Then Eq. (C.42) is satisfied when

$$G_a = G_b. \tag{C.44}$$

We proceed as previously, substituting standard wave expressions in Eq. (C.44), truncating the sums, multiplying by $\frac{1}{g_{2n}r}U_n(r)$ for each n, $n = 1, \cdots, N_3$, and integrating over dr from r_H to r_D, where

$$g_{2n} = \int_{r_H}^{r_D} U_n^2(r)dr\,. \tag{C.45}$$

We obtain the result

$$\sum_{n'=1}^{N_1} G^a_{1sknn'}A^a_{1skn'} - \sum_{n'=1}^{N_2} G^b_{2sknn'}A^b_{2skn'} - \sum_{n'=1}^{N_3} G^b_{3sknn'}A^b_{3skn'}$$
$$= \sum_{n'=1}^{N_1} G^b_{1sknn'}A^b_{1skn'} - \sum_{n'=1}^{N_2} G^a_{2sknn'}A^a_{2skn'} - \sum_{n'=1}^{N_3} G^a_{3sknn'}A^a_{3skn'}, \tag{C.46}$$
$$n = 1, \cdots, N_3,$$

where

$$G^P_{1sknn'} = -\delta_{2n,n'}mc_P\frac{M_P}{\lambda^P_{1skn'}} + \delta_{3n,n'}M_{sP}c_P\frac{\gamma^P_{1skn'}}{\lambda^P_{1skn'}}, \tag{C.47}$$

$$G^P_{2sknn'} = -\delta_{2n,n'}mc_P\frac{M_P}{\lambda^P_{2skn'}} + \delta_{3n,n'}M_{sP}c_P\frac{\gamma^P_{2skn'}}{\lambda^P_{2skn'}}, \tag{C.48}$$

$$G^P_{3sknn'} = \delta_{n,n'}\left(1.4\frac{p_P}{p_\infty}\frac{a_\infty}{c_P}M_P\gamma^P_{3skn'} + 1.4\frac{p_P}{p_\infty}\frac{a_\infty}{c_P}mM_{sP}\right) \tag{C.49}$$

for $P = a$ or b, and

$$\delta_{2n,n'} = \frac{1}{g_{2n}}\int_{r_H}^{r_D}\frac{1}{r^2}\Psi_{m'n'}(r)U_n(r)dr\,, \tag{C.50}$$

$$\delta_{3n,n'} = \frac{1}{g_{2n}}\int_{r_H}^{r_D}\Psi_{m'n'}(r)U_n(r)dr\,. \tag{C.51}$$

In the above, $M_{sP} = \Omega_{sP} r_D / c_P$, the swirl Mach number at the outer duct radius.

Matrix Equation

Let C_1^a be the matrix consisting of all elements $C^a_{1sknn_i}$ for all allowable s, k, n, and n_i. Let C_1^b, C_2^a, C_2^b, C_3^a, C_3^b, F_1^a, F_1^b, F_2^a, F_2^b, F_3^a, F_3^b, G_1^a, G_1^b, G_2^a, G_2^b, G_3^a, and G_3^b be defined analogously. Then Eqs. (C.29), (C.37), and (C.46) can be combined and written in matrix form as

$$K_{out} A_{out} = K_{in} A_{in}, \tag{C.52}$$

where

$$K_{out} = \begin{bmatrix} C_1^a & -C_2^b & -C_3^b \\ F_1^a & -F_2^b & -F_3^b \\ G_1^a & -G_2^b & -G_3^b \end{bmatrix}, \tag{C.53}$$

$$K_{in} = \begin{bmatrix} C_1^b & -C_2^a & -C_3^a \\ F_1^b & -F_2^a & -F_3^a \\ G_1^b & -G_2^a & -G_3^a \end{bmatrix}, \tag{C.54}$$

$$A_{out} = \begin{Bmatrix} A_1^a \\ A_2^b \\ A_3^b \end{Bmatrix}, \tag{C.55}$$

$$A_{in} = \begin{Bmatrix} A_1^b \\ A_2^a \\ A_3^a \end{Bmatrix}. \tag{C.56}$$

The vectors A_{out} and A_{in} consist, respectively, of output and input state vectors of type A_W^P; the vectors A_W^P have been defined earlier in Section 2.2.

Eq. (C.52) can be solved to give

$$\begin{aligned} A_{out} &= K_{out}^{-1} K_{in} A_{in} \\ &= K_{io} A_{in}, \end{aligned} \tag{C.57}$$

where

$$K_{io} = K_{out}^{-1} K_{in}. \tag{C.58}$$

Clearly the elements of K_{io} give the ratios of the output to the input state vector coefficients. By the definition of scattering coefficients, this means that K_{io} is the scattering matrix for the actuator disk. This result is for input and output waves originating at the actuator disk. After these locations are shifted axially, in Section 4.1, we obtain the final matrix.

APPENDIX D

COMBINING STATOR OR ROTOR WITH AN ACTUATOR DISK

The source vector coefficients and scattering coefficients for the stator alone and scattering coefficients for the actuator disk have been derived separately for the configurations shown in Fig. D.1a. In this figure, each A_W^P represents the vector made up of all components A_{Wskn}^P of type W at interface P over all allowable values of the indices s, k, n. The quantities B_W^P are defined analogously for source vectors. See Section 2.2 for a more detailed description of these vectors. In this appendix, we derive the scattering coefficients and source vector coefficients for the combined stator/actuator disk element shown in Fig. D.1b. Afterwards we will discuss a combined element for the rotor. Note that the indices for the interface locations in Fig. D.1 are kept general, i.e. a, b, and c, so that similar notation can be used later for the rotor/actuator disk situation. Then rotor results will be analogous to stator results. Referring to Fig. 3.1, we see that for the stator/actuator disk case, $x^a = x^2$, $x^b = x^e$, and $x^c = x^3$. The analysis here was developed jointly with D. Hanson.

Referring to Fig. D.1a, we can write for the stator

$$A_1^a = S_{12}^{aa} A_2^a + S_{13}^{aa} A_3^a + S_{11}^{ab} A_1^b + B_1^a, \tag{D.1}$$

$$A_2^b = S_{22}^{ba} A_2^a + S_{23}^{ba} A_3^a + S_{21}^{bb} A_1^b + B_2^b, \tag{D.2}$$

$$A_3^b = S_{32}^{ba} A_2^a + S_{33}^{ba} A_3^a + S_{31}^{bb} A_1^b + B_3^b, \tag{D.3}$$

where we have equated standard waves on the left with their component parts on the right. Exponential and other factors, that would be present in the standard wave representations, are omitted because they cancel from both sides. In the above, the quantities $S_{WW_i}^{PP_i}$, defined in Section 2.2, denote the scattering matrices made up of all the scattering coefficient elements $S_{WW_i skn;sk_in_i}^{PP_i}$ for the stator alone whose indices fall in the range of values allowed. The A_W^P's on the left of the equations are for output waves; those on the right are for input ones.

For the actuator disk, we have similarly

$$A_1^b = S_{12}^{bb} A_2^b + S_{13}^{bb} A_3^b + S_{11}^{bc} A_1^c, \tag{D.4}$$

$$A_2^c = S_{22}^{cb} A_2^b + S_{23}^{cb} A_3^b + S_{21}^{cc} A_1^c, \tag{D.5}$$

$$A_3^c = S_{32}^{cb} A_2^b + S_{33}^{cb} A_3^b + S_{31}^{cc} A_1^c, \tag{D.6}$$

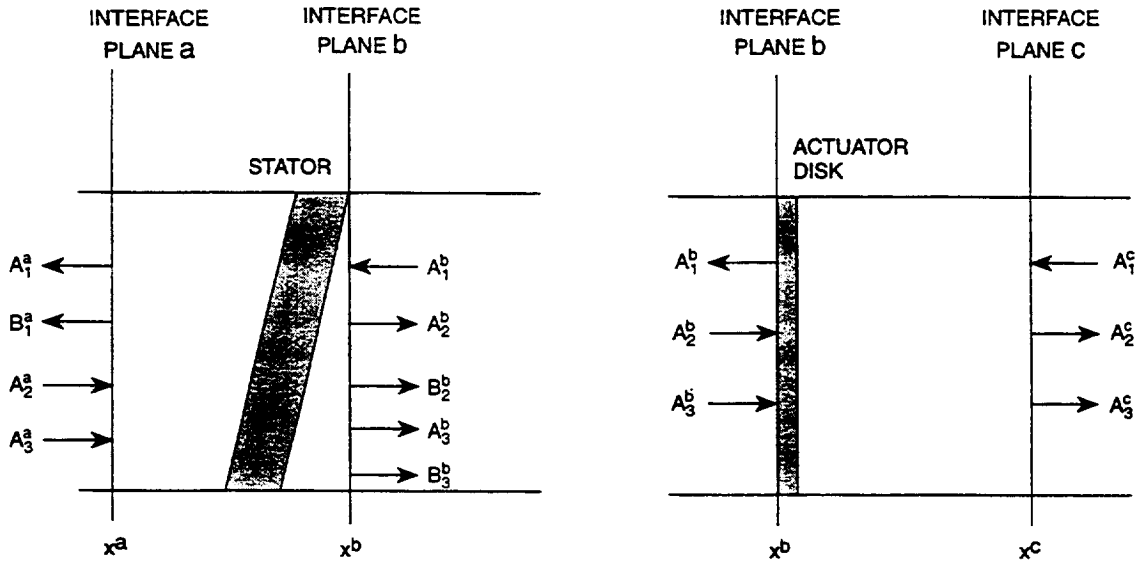

(A) STATOR AND ACTUATOR DISK AS SEPARATE ELEMENTS

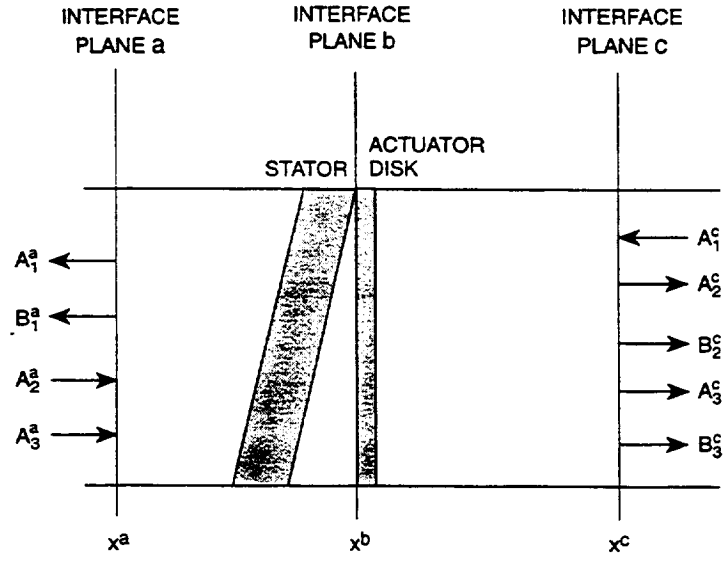

(B) STATOR AND ACTUATOR DISK AS ONE ELEMENT

FIGURE D.1 COMBINING THE STATOR ALONE AND ACTUATOR DISK INTO ONE ELEMENT

where the scattering coefficient elements $S^{PP_i}_{WW_i;skn;skn_i}$ in the scattering matrices $S^{PP_i}_{WW_i}$ above are those for the actuator disk. Again, the A^P_W's on the left are for output waves, those on the right for input ones.

Eqs. (D.1)-(D.6) can be written in block matrix form as

$$\begin{Bmatrix} A^a \\ A^b \\ A^c \end{Bmatrix}_{out} = \begin{bmatrix} S^{aa} & S^{ab} & \cdot \\ S^{aa} & S^{bb} & S^{bc} \\ \cdot & S^{cb} & S^{cc} \end{bmatrix} \begin{Bmatrix} A^a \\ A^b \\ A^c \end{Bmatrix}_{in} + \begin{Bmatrix} B^a \\ B^b \\ B^c \end{Bmatrix}, \tag{D.7}$$

where

$$A^P = \begin{Bmatrix} A^P_1 \\ A^P_2 \\ A^P_3 \end{Bmatrix}, \quad B^P = \begin{Bmatrix} B^P_1 \\ B^P_2 \\ B^P_3 \end{Bmatrix}, \quad S^{aa} = \begin{bmatrix} \cdot & S^{aa}_{12} & S^{aa}_{13} \\ \cdot & \cdot & \cdot \\ \cdot & \cdot & \cdot \end{bmatrix}, \quad S^{ab} = \begin{bmatrix} S^{ab}_{11} & \cdot & \cdot \\ \cdot & \cdot & \cdot \\ \cdot & \cdot & \cdot \end{bmatrix},$$

$$S^{ba} = \begin{bmatrix} \cdot & \cdot & \cdot \\ \cdot & S^{ba}_{22} & S^{ba}_{23} \\ \cdot & S^{ba}_{32} & S^{ba}_{33} \end{bmatrix}, \quad S^{bb} = \begin{bmatrix} \cdot & S^{bb}_{12} & S^{bb}_{13} \\ S^{bb}_{21} & \cdot & \cdot \\ S^{bb}_{31} & \cdot & \cdot \end{bmatrix}, \quad S^{bc} = \begin{bmatrix} S^{bc}_{11} & \cdot & \cdot \\ \cdot & \cdot & \cdot \\ \cdot & \cdot & \cdot \end{bmatrix}, \tag{D.8}$$

$$S^{cb} = \begin{bmatrix} \cdot & \cdot & \cdot \\ \cdot & S^{cb}_{22} & S^{cb}_{23} \\ \cdot & S^{cb}_{32} & S^{cb}_{33} \end{bmatrix}, \quad S^{cc} = \begin{bmatrix} \cdot & \cdot & \cdot \\ S^{cc}_{21} & \cdot & \cdot \\ S^{cc}_{31} & \cdot & \cdot \end{bmatrix}.$$

In the matrices above, the dots denote zero matrices. The notations $\{\ \}_{in}$ and $\{\ \}_{out}$ in Eq. (D.7) designate, respectively, input and output waves.

Eq. (D.7) can be rewritten in the alternate matrix form as

$$A^a_{out} = S^{aa} A^a_{in} + S^{ab} A^b_{in} \qquad + B^a, \tag{D.9}$$

$$A^b_{out} = S^{ba} A^a_{in} + S^{bb} A^b_{in} + S^{bc} A^c_{in} + B^b, \tag{D.10}$$

$$A^c_{out} = \qquad S^{cb} A^b_{in} + S^{cc} A^c_{in} + B^c, \tag{D.11}$$

where we have changed the A^P's from Eq. (D.7) to A^P_{in}'s and A^P_{out}'s to indicate whether they came, respectively, from the input or the output vectors there.

To obtain the scattering matrix and source vector for the combined element case of Fig. D.1b, we must eliminate the A_{in}^{b}'s and A_{out}^{b}'s from Eqs. (D.9)-(D.11). To do this, note that, for the combined element, the output waves in Fig. D.1a in the region between the stator and the actuator disk must be the same as the input waves going into the actuator disk there. Similarly, the output waves traveling from the actuator disk to the stator must be the same as the input waves entering the stator there. Hence, we require $A_{in}^{b} = A_{out}^{b}$. Let us set $A^{b} = A_{in}^{b} = A_{out}^{b}$, then Eq. (D.10) gives that

$$(1 - S^{bb})A^{b} = S^{ba}A_{in}^{a} + S^{bc}A_{in}^{c} + B^{b}, \tag{D.12}$$

so

$$A^{b} = ES^{ba}A_{in}^{a} + ES^{bc}A_{in}^{c} + EB^{b}, \tag{D.13}$$

where

$$E = (1 - S^{bb})^{-1}. \tag{D.14}$$

Using Eq. (D.13) in Eqs. (D.9) and (D.11), then

$$A_{out}^{a} = (S^{aa} + S^{ab}ES^{ba})A_{in}^{a} + S^{ab}ES^{bc}A_{in}^{c} + S^{ab}EB^{b} + B^{a}, \tag{D.15}$$

$$A_{out}^{c} = S^{cb}ES^{ba}A_{in}^{a} + (S^{cc} + S^{cb}ES^{bc})A_{in}^{c} + S^{cb}EB^{b} + B^{c}. \tag{D.16}$$

Hence,

$$\begin{Bmatrix} A^{a} \\ A^{c} \end{Bmatrix}_{out} = \begin{bmatrix} [S^{aa} + S^{ab}ES^{ba}] & [S^{ab}ES^{bc}] \\ [S^{cb}ES^{ba}] & [S^{cc} + S^{cb}ES^{bc}] \end{bmatrix} \begin{Bmatrix} A^{a} \\ A^{c} \end{Bmatrix}_{in} + \begin{Bmatrix} \{B^{a} + S^{ab}EB^{b}\} \\ \{B^{c} + S^{cb}EB^{b}\} \end{Bmatrix}. \tag{D.17}$$

Taking the two state vectors above as A_{out} and A_{in}, and setting

$$S_{COMB} = \begin{bmatrix} [S^{aa} + S^{ab}ES^{ba}] & [S^{ab}ES^{bc}] \\ [S^{cb}ES^{ba}] & [S^{cc} + S^{cb}ES^{bc}] \end{bmatrix}, \tag{D.18}$$

$$B_{COMB} = \begin{Bmatrix} \{B^{a} + S^{ab}EB^{b}\} \\ \{B^{c} + S^{cb}EB^{b}\} \end{Bmatrix}, \tag{D.19}$$

we have, finally,

$$A_{out} = S_{COMB}A_{in} + B_{COMB}. \tag{D.20}$$

When $B_{COMB} = 0$, we see that the elements of S_{COMB} provide the ratios of the output to the input state vector coefficients. Therefore, by the definition of scattering coefficients, S_{COMB} is the

scattering matrix for the combined element. Also, clearly, B_{COMB} is the source vector for the combined element.

The derivation for the rotor case is similar. In place of Fig. D.1, we now use Fig. D.2 to obtain the equations

$$A_1^a = S_{12}^{aa} A_2^a + S_{13}^{aa} A_3^a + S_{11}^{ab} A_1^b , \tag{D.21}$$

$$A_2^b = S_{22}^{ba} A_2^a + S_{23}^{ba} A_3^a + S_{21}^{bb} A_1^b , \tag{D.22}$$

$$A_3^b = S_{32}^{ba} A_2^a + S_{33}^{ba} A_3^a + S_{31}^{bb} A_1^b , \tag{D.23}$$

$$A_1^b = S_{12}^{bb} A_2^b + S_{13}^{bb} A_3^b + S_{11}^{bc} A_1^c , \tag{D.24}$$

$$A_2^c = S_{22}^{cb} A_2^b + S_{23}^{cb} A_3^b + S_{21}^{cc} A_1^c , \tag{D.25}$$

$$A_3^c = S_{32}^{cb} A_2^b + S_{33}^{cb} A_3^b + S_{31}^{cc} A_1^c . \tag{D.26}$$

These equations have the same form as Eqs. (D.1)-(D.6) have for the stator case, only source vector terms are no longer present and $x^a = x^1$, $x^b = x^i$, and $x^c = x^2$. This change in x^a, x^b, and x^c means that rotor alone coefficients replace the actuator disk coefficients in Eqs. (D.1)-(D.6), and actuator disk coefficients replace the stator alone ones.

Proceeding from this point on, exactly as before, we now obtain

$$A_{out} = S_{COMB} A_{in} \tag{D.27}$$

in place of Eq. (D.20), where S_{COMB} is given by Eq. (D.18). We see, again, that the elements of S_{COMB} provide the ratios of the output to the input state vector coefficients. Hence, S_{COMB} is the scattering matrix for the combined element. The quantities S^{aa}, S^{ab}, S^{ba}, S^{bc}, S^{cb}, S^{cc}, and E in Eq. (D.18) are, again, specified by Eqs. (D.8) and (D.14), only now the change in x^a, x^b, and x^c gives elements that are different from those for the stator case.

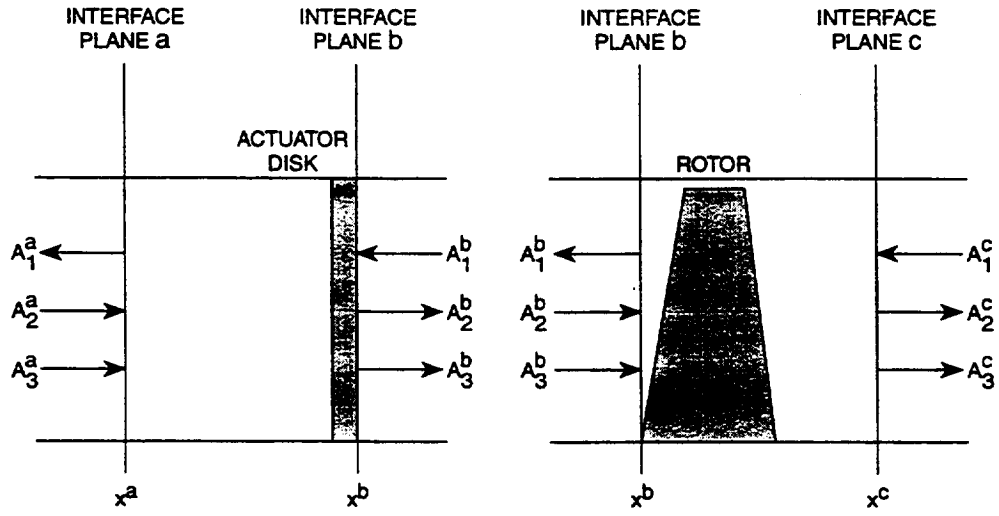

(A) ROTOR AND ACTUATOR DISK AS SEPARATE ELEMENTS

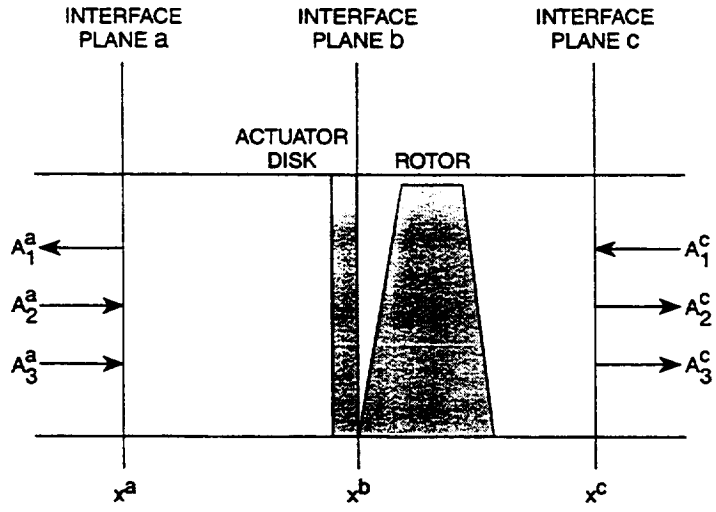

(B) ROTOR AND ACTUATOR DISK AS ONE ELEMENT

FIGURE D.2 COMBINING THE ROTOR ALONE AND ACTUATOR DISK INTO ONE ELEMENT

REFERENCES

1. Meyer, H. D. and E. Envia, "Acoustic Analysis of Turbofan Noise Generation," NASA CR-4715, March 1996.

2. Topol, D. A., S. C. Holhubner, and D. C. Mathews, "A Reflection Mechanism for Aft Fan Tone Noise," AIAA Paper 87-2699, October 1987.

3. Hanson, D. B., Mode Trapping in Coupled 2D Cascades - Acoustic and Aerodynamic Results," AIAA Paper 93-4417, October 1993.

4. Meyer, H. D., "Effect of Inlet Reflections on Fan Noise Radiation," *AIAA Journal*, Vol. 34, No. 9, September 1996, pp.1771-1777.

5. Topol, D. A., TFaNS Theoretical Fan Noise Design/Prediction System, Volume 1: System Description, CUP3D Technical Documentation and Manual for Code Developers," NASA CR, 1997.

6. Smith, S. N., "Discrete Frequency Sound Generation in Axial Flow Turbomachines," Aeronautical Research Council Reports and Memoranda, No. 3709, March 1972.

7. Golubev, V. V. and H. M. Atassi, "Sound Propagation in an Annular Duct with Mean Potential Swirling Flow," *Journal of Sound and Vibration*, Vol. 198, No. 5, December 1996, pp. 601-616.

8. Goldstein, M. E., *Aeroacoustics*, McGraw-Hill, New York, 1976.

9. Majjigi, R. K. and P. R. Gliebe, "Development of a Rotor Wake/Vortex Model, Volume 1: Final Report," NASA CR-174849, June 1984.

10. Topol, D. A. and D. A. Philbrick, "Fan Noise Prediction System Development: Wake Model Improvements and Code Evaluations," NASA Contract No. NAS3-25952 (Task 10) Report, April 1993.

11. Hanson, D. B., "Acoustic Reflection and Transmission of 2-Dimensional Rotors and Stators, Including Mode and Frequency Scattering Effects," NASA CR, 1997.

12. Meyer, H. D., "Acoustic Scattering by Three-Dimensional Stators and Rotors Using the SOURCE3D Code, Volume 1: Analysis and Results," NASA CR, 1997.

13. Ventres, C. S., M. A. Theobold, and W. D. Mark, "Turbofan Noise Generation, Volume 1: Analysis," NASA CR-167951, July 1982.

14. Hanson, D. B., "Coupled 2-Dimensional Cascade Theory for Noise and Unsteady Aerodynamics of Blade Row Interaction in Turbofans, Volume 1 – Theory Development and Parametric Studies," NASA CR-4506, October 1993.

ACKNOWLEDGMENTS

The author would like to thank Donald B. Hanson and David A. Topol of Pratt & Whitney for their helpful suggestions and critiques. Also, appreciation is due to Donald B. Hanson for suggesting this project and for his contributions to theory which have been acknowledged in the text where appropriate. Additionally, thanks should be given to Dennis L. Huff of NASA Lewis Research Center for his support.

REPORT DOCUMENTATION PAGE

Form Approved
OMB No. 0704-0188

1. AGENCY USE ONLY (*Leave blank*)	2. REPORT DATE	3. REPORT TYPE AND DATES COVERED
	March 1999	Final Contractor Report

4. TITLE AND SUBTITLE

Source Methodology for Turbofan Noise Prediction
(SOURCE3D Technical Documentation)

5. FUNDING NUMBERS

WU–538–03–11–00
NAS3–26618

6. AUTHOR(S)

Harold D. Meyer

7. PERFORMING ORGANIZATION NAME(S) AND ADDRESS(ES)

United Technologies Corporation
Hamilton Standard Division
1 Hamilton Road
Windsor Locks, Connecticut 06096

8. PERFORMING ORGANIZATION REPORT NUMBER

E–11581
PWA 6420–104

9. SPONSORING/MONITORING AGENCY NAME(S) AND ADDRESS(ES)

National Aeronautics and Space Administration
John H. Glenn Research Center at Lewis Field
Cleveland, Ohio 44135–3191

10. SPONSORING/MONITORING AGENCY REPORT NUMBER

NASA CR—1999-208877

11. SUPPLEMENTARY NOTES

Project Manager, Dennis L. Huff, NASA Lewis Research Center, organization code 5940, (216) 433–3913.

12a. DISTRIBUTION/AVAILABILITY STATEMENT

Unclassified - Unlimited
Subject Category: 71 Distribution: Standard

This publication is available from the NASA Center for AeroSpace Information, (301) 621–0390.

12b. DISTRIBUTION CODE

13. ABSTRACT ***(Maximum 200 words)***

This report provides the analytical documentation for the SOURCE3D Rotor Wake/Stator Interaction Code. It derives the equations for the rotor scattering coefficients and stator source vector and scattering coefficients that are needed for use in the TFaNS (Theoretical Fan Noise Design/Prediction System). SOURCE3D treats the rotor and stator as isolated source elements. TFaNS uses this information, along with scattering coefficients for inlet and exit elements, and provides complete noise solutions for turbofan engines. SOURCE3D is composed of a collection of FORTRAN programs that have been obtained by extending the approach of the earlier V072 Rotor Wake/Stator Interaction Code. Similar to V072, it treats the rotor and stator as a collection of blades and vanes having zero thickness and camber contained in an infinite, hardwall annular duct. SOURCE3D adds important features to the V072 capability—a rotor element, swirl flow and vorticity waves, actuator disks for flow turning, and combined rotor/actuator disk and stator/actuator disk elements. These items allow reflections from the rotor, frequency scattering, and mode trapping, thus providing more complete noise predictions than previously. The code has been thoroughly verified through comparison with D.B. Hanson's CUP2D two-dimensional code using a narrow annulus test case.

14. SUBJECT TERMS

Acoustics; Turbomachinery; Noise; Fans

15. NUMBER OF PAGES

84

16. PRICE CODE

A05

17. SECURITY CLASSIFICATION OF REPORT	18. SECURITY CLASSIFICATION OF THIS PAGE	19. SECURITY CLASSIFICATION OF ABSTRACT	20. LIMITATION OF ABSTRACT
Unclassified	Unclassified	Unclassified	